

1 Convergent network effects along the axis of 2 gene expression during prostate cancer 3 progression

4 Konstantina Charmpi^{1,2,✉}, Tiannan Guo^{3,4,5,✉,*}, Qing Zhong^{6,✉}, Ulrich Wagner^{6,✉}, Rui Sun^{4,5}, Nora C.
5 Toussaint^{6,7,8}, Christine E. Fritz⁶, Chunhui Yuan^{4,5}, Hao Chen^{4,5}, Niels J. Rupp⁶, Ailsa Christiansen⁶,
6 Dorothea Rutishauser⁶, Jan H. Rüschoff⁶, Christian Fankhauser⁶, Karim Saba^{6,9}, Cedric Poyet⁹, Thomas
7 Hermanns⁹, Kathrin Oehl⁶, Ariane L. Moore¹⁰, Christian Beisel¹⁰, Laurence Calzone¹¹, Loredana
8 Martignetti¹¹, Qiushi Zhang^{4,5}, Yi Zhu^{3,4,5}, María Rodríguez Martínez¹², Matteo Manica¹², Michael C.
9 Haffner¹³, Ruedi Aebersold^{3,14,*}, Peter J. Wild^{6,15,*}, Andreas Beyer^{1,2,*}

10

11 ¹ CECAD, University of Cologne, Cologne, Germany

12 ² Center for Molecular Medicine Cologne (CMMC), Medical Faculty, University of Cologne, Cologne,
13 Germany

14 ³ Department of Biology, Institute of Molecular Systems Biology, ETH Zurich, Zurich, Switzerland

15 ⁴ Zhejiang Provincial Laboratory of Life Sciences and Biomedicine, Key Laboratory of Structural Biology of
16 Zhejiang Province, School of Life Sciences, Westlake University, Hangzhou 310024, China

17 ⁵ Institute of Basic Medical Sciences, Westlake Institute for Advanced Study, Hangzhou 310024, China

18 ⁶ Department of Pathology and Molecular Pathology, University Hospital Zurich, University of Zurich,
19 Zurich, Switzerland

20 ⁷ NEXUS Personalized Health Technologies, ETH Zurich, Zurich, Switzerland

21 ⁸ Swiss Institute of Bioinformatics, Zurich, Switzerland

22 ⁹ Department of Urology, University Hospital Zurich, University of Zurich, Zurich, Switzerland

23 ¹⁰ Department of Biosystems Science and Engineering, ETH Zurich, Basel, Switzerland

24 ¹¹ Institut Curie, Paris, France

25 ¹² IBM Zurich Research Laboratory, Zurich, Switzerland

26 ¹³ Fred Hutchinson Cancer Research Center, Seattle, USA

27 ¹⁴ Faculty of Science, University of Zurich, Zurich, Switzerland

28 ¹⁵ Dr. Senckenberg Institute of Pathology, University Hospital Frankfurt, Goethe-University Frankfurt,
29 Frankfurt, Germany.

30

31

32 *Corresponding authors:

33 Tiannan Guo: guotiannan@westlake.edu.cn

34 Ruedi Aebersold: aebersold@imsb.biol.ethz.ch

35 Peter J. Wild: Peter.Wild@kgu.de

36 Andreas Beyer: abeyer2@uni-koeln.de

37 [✉]Equal contribution

38 **Abstract**

39 **Background**

40 Tumor-specific genomic aberrations are routinely determined by high throughput genomic
41 measurements. It remains unclear though, how complex genome alterations affect molecular networks
42 through changing protein levels, and consequently biochemical states of tumor tissues.

43 **Results**

44 Here, we investigated the propagation of genomic effects along the axis of gene expression during
45 prostate cancer progression. For that, we quantified genomic, transcriptomic and proteomic alterations
46 based on 105 prostate samples, consisting of benign prostatic hyperplasia regions and malignant tumors,
47 from 39 prostate cancer patients. Our analysis revealed convergent effects of distinct copy number
48 alterations impacting on common downstream proteins, which are important for establishing the tumor
49 phenotype. We devised a network-based approach that integrates perturbations across different
50 molecular layers, which identified a sub-network consisting of nine genes whose joint activity positively
51 correlated with increasingly aggressive tumor phenotypes and was predictive of recurrence-free survival.
52 Further, our data revealed a wide spectrum of intra-patient network effects, ranging from similar to very
53 distinct alterations on different molecular layers.

54 **Conclusions**

55 This study uncovered molecular networks with remarkably convergent alterations across tumor sites and
56 patients, but it also exposed a diversity of network effects: we could not identify a single sub-network
57 that was perturbed in all high-grade tumor regions.

58

59 **Keywords:** molecular aberrations, network effects, prostate cancer, proteogenomic analysis, tumor
60 heterogeneity

61

62 **Background**

63 Prostate cancer (PCa) represents one of the most common neoplasms among men with almost
64 1,300,000 new cases and 360,000 deaths in 2018 ¹ accounting for 15% of all cancers diagnosed. PCa is
65 the fifth leading cause of cancer death in men and represents 6.6% of total cancer mortality in men [1].
66 Despite earlier detection and new treatments, the lifetime risk to die of PCa has remained stable at
67 approximately 3% since 1980. (National Cancer Institute SEER data:
68 <https://seer.cancer.gov/statfacts/html/prost.html>). In many patients, PCa is indolent and slowly growing.
69 The challenge is to identify those patients who are unlikely to experience significant progression while
70 offering radical therapy to those who are at risk. Current risk stratification models are based on
71 clinicopathological variables including histomorphologically defined grade groups, prostate-specific
72 antigen (PSA) levels and clinical stage. Although those variables provide important information for
73 clinical risk assessment and treatment planning [2, 3], they do not sufficiently predict the course of the
74 disease.

75 Extensive genomic profiling efforts have provided important insights into the common genomic
76 alterations in primary and metastatic PCa [4-9]. Interestingly, PCa genomes show a high frequency of
77 recurrent large-scale chromosomal rearrangements such as TMPRSS2-ERG [10]. In addition, extensive
78 copy number alterations (CNAs) are common in PCa, yet point mutations are relatively infrequent in
79 primary PCa compared to other cancers [6, 11]. A major complicating factor is that around 80% of PCas
80 are multifocal and harbor multiple spatially and often morphologically distinct tumor foci [12, 13].
81 Several recent studies have suggested that the majority of topographically distinct tumor foci appear to
82 arise independently and show few or no overlap in driver gene alterations [14-16]. Therefore, a given
83 prostate gland can harbor clonally independent PCas.

84 To allow for a more functional assessment of the biochemical state of PCa, it is necessary to go
85 beyond genomic alterations and comprehensively catalogue cancer specific genomic, transcriptomic and
86 proteomic alterations in an integrated manner [17-19]. Such an approach will provide critical
87 information for basic and translational research and could result into clinically relevant markers. While
88 hundreds of PCa genomes and transcriptomes have been profiled to date [20], little is known about the
89 PCa proteome. Although recent work has emphasized the need for integrated multi-omics profiling of
90 PCa, we still lack understanding about how genomic changes impact on mRNA and protein levels [17-19].
91 Especially the complex relationship between tumor grade, tumor progression and multi-layered
92 molecular network changes remains largely elusive.

93 For example, previous work has shown that copy number changes may alter transcript levels of
94 many genes, whereas the respective protein levels remain relatively stable [21]. Indeed, there is
95 compelling evidence across multiple tumor types that many genomic alterations are ‘buffered’ at the
96 protein level and are hence mostly clinically inconsequential [22]. To better understand the evolution of
97 PCa and to identify core networks perturbed by genomic alterations and thus central for the tumor
98 phenotype, it is therefore essential to investigate the transmission of CNAs to the transcriptomic and
99 proteomic level.

100 To this end, it is important to decipher which genomic alterations impact PCa proteomes, which
101 of those proteomic alterations are functionally relevant, and how molecular networks are perturbed at
102 the protein level across tumors.

103 To address these open questions, we performed a multi-omics profiling of radical prostatectomy
104 (RP) specimens at the level of the genome, transcriptome and proteome from adjacent biopsy-level
105 samples, using state-of-the-art technologies. Unique features of this study are (1) the utilization of PCT
106 (pressure cycling technology)-SWATH (Sequential Window Acquisition of all Theoretical Mass Spectra)
107 mass spectrometry [23, 24], allowing rapid and reproducible quantification of thousands of proteins
108 from biopsy-level tissue samples collected in clinical cohorts; (2) the simultaneous profiling of all omics
109 layers from the same tissue regions; (3) inclusion and full profiling of benign regions, which provides a
110 matching control for each tumor; and (4) the full multi-omics characterization of multiple tumor regions
111 from the same patients, thus enabling the detailed investigation of tumor heterogeneity. This design
112 resulted in the multi-layered analyses of 105 samples from 39 PCa patients, as well as of the exome of
113 corresponding peripheral blood cells yielding a comprehensive molecular profile for each patient and
114 identified molecular networks that are commonly altered in multiple patients. Importantly, some of the
115 affected genes/proteins exhibited very small individual effect sizes, suggesting that combined network
116 effects of multiple genes may significantly contribute to determining PCa phenotypes.

117 **Results**

118 **Proteogenomic analysis of the sample cohort identifies known PCa biomarkers.**

119 In this study, we analyzed 39 PCa patients (**Additional file 1: Fig. S1**) belonging to three groups
120 who underwent laparoscopic robotic-assisted RP. The patients were from the PCa Outcomes Cohort
121 (ProCOC) study [25, 26]. Tumor areas were graded using the ISUP (International Society of Urological
122 Pathology) grade groups [27], which range from ISUP grade group G1 (least aggressive) to G5 (most

123 aggressive). The more advanced grade groups G4 and G5 were considered jointly (G4/5). The cohort
124 tested included 12 low-grade (G1), 17 intermediate- (G2 and G3), and 10 high-grade (G4/5) patients (**Fig.**
125 **1a, Additional file 1: Fig. S1, Additional file 2: Table S1**). For low-grade PCa patients, we selected two
126 representative regions, one of benign prostatic hyperplasia (BPH) and one of malignant tumor (TA). Since
127 PCa often presents as a multifocal disease with heterogeneous grading within each prostate specimen
128 [24] we analyzed two different tumor regions from the 27 intermediate- and high-grade patients. In
129 those cases three representative regions, including BPH, the most aggressive tumor (TA1) and a
130 secondary, lower-grade tumor (TA2) [2] were analyzed. Thus, TA1 always represented the higher-grade
131 nodule compared to TA2. Note, whereas each patient was assigned a patient-specific overall grade (*i.e.*
132 ‘low’, ‘intermediate’ or ‘high’), each tumor area was additionally assigned an individual grade group
133 based on its histological appearance. According to current ISUP guidelines, the grading of the entire
134 prostate specimen depends on the size and grade of individual nodules [28]. Thus, it is possible that the
135 patient grading is lower than the grading of the most aggressive nodule, if another lower-grade nodule is
136 larger. Tumor regions contained at least 70% tumor cellularity and the distance between the analyzed
137 areas (TA1 versus TA2) was at least 5 mm. Altogether, we obtained 105 prostate tissue specimens
138 (**Additional file 2: Table S1**). Three adjacent tissue biopsies of the dimensions 0.6 x 0.6 x 3.0 mm were
139 punched from each representative region for exome sequencing, CNA (derived from the exome
140 sequencing data), RNA sequencing (RNA-seq), and quantitative proteomic analysis using the PCT-SWATH
141 technology [23] respectively. Proteomic analysis was performed in duplicates for each tissue sample.
142 Peripheral blood samples from each patient were also subjected to exome sequencing and served as the
143 genomic wild-type reference (**Fig. 1**). All three types of grading (*i.e.* patient-specific overall grading, TA1
144 grading and TA2 grading) were predictive of the recurrence-free survival (RFS) in our study.

145 In agreement with prior reports, we observed relatively few recurrent point mutations across
146 patients (**Additional file 1: Fig. S2, Additional file 3: Table S2**), but substantial CNAs (**Additional file 1:**
147 **Figs. S3 and S4, Additional file 4: Table S3**). Mutations in SPOP, FOXA1, and MED12 reported in
148 independent cohorts [4-9] were confirmed in this cohort. In total, 1,110 genes showed copy number
149 gains in at least five samples or copy number losses in at least five samples (see **Additional file 1:**
150 **Supplementary Text** for details). **Additional file 1: Fig. S4** shows the CNA status of signature genes
151 representing known areas of recurrent CNAs in PCa- split into fusion-partner and non-fusion-partner
152 genes- for instance loss of PTEN and gain of MYC in high-grade PCa [29]. Likewise, our data confirmed
153 the differential expression of several transcripts/proteins that had previously been suggested as PCa
154 biomarkers or which are known oncogenes in other tumor types (**Additional file 1: Supplementary Text**

155 **and Fig. S5, Additional file 5: Table S4 and Additional file 6: Table S5**). We further identified somatic
156 fusions from the RNA-seq data. A large fraction of the tumors harbored ETS family gene fusions, which
157 are frequently detected in PCa [8, 9, 11]. ETS fusions were mutually exclusive and appeared in tumors
158 from all grade groups (**Additional file 1: Fig. S6; Additional file 5: Table S4**). This consistency with
159 previously published results confirmed the quality of our data and motivated us to go beyond previous
160 work by performing a network-based multi-omics multi-gene analysis.

161 **Molecular perturbations correlate with tumor grade.**

162 Mutational burden is associated with PCa risk [8, 9, 11]. Hence, as a first step towards a cross-
163 layer analysis, we asked if high-grade PCa would generally be affected by stronger alterations (compared
164 to low-grade PCa) at the genome, transcriptome, and proteome layer [30]. For that purpose, we devised
165 molecular perturbation scores that quantified the number of affected genes/proteins and the extent to
166 which these genes/proteins were altered in the tumor specimens compared to their benign controls (see
167 the '**Methods**' section for details). In the case of the DNA layer these scores carry a similar meaning as
168 established mutational burden scores. However, we wanted to capture effects at all three molecular
169 layers measured in this study. Higher-grade tumors (G3 and G4/5) exhibited significantly higher
170 molecular perturbation scores than lower-grade tumors (G1 and G2). Those differences were statistically
171 significant in all but one case (P value < 0.05 , one-sided Wilcoxon rank sum test, **Fig. 2**). The CNA
172 perturbation magnitude exhibited the highest correlation with the PCa grading, confirming prior studies
173 documenting the tight association between CNA, histopathological grade and risk of progression [4, 5,
174 31]. Further, we found that mRNA fold changes (FCs) correlated more strongly with CNAs of the same
175 genes than protein FCs (average CNA-mRNA Spearman $\rho = 0.1$ and average CNA-protein Spearman $\rho =$
176 0.02). This observation is in agreement with previous work, which suggested that copy number changes
177 are to some extent buffered at the protein level [17, 21, 32]. Interestingly, we observed that proteins
178 known to be part of protein complexes were significantly less strongly correlated with the FCs of their
179 coding mRNAs than proteins not known to be part of protein complexes (P value $< 2.6\text{e-}11$, one-sided t-
180 test, **Additional file 1: Fig. S7**). This result is consistent with the concept that protein complex
181 stoichiometry contributes to the buffering of mRNA changes at the level of proteins [21, 22, 33-35]. Thus,
182 molecular patterns in high-grade PCa are more strongly perturbed at all layers and the effects of
183 genomic variation are progressively but non-uniformly attenuated along the axis of gene expression.

184 **Effects of distinct CNAs converge on common proteins.**

185 It has previously been suggested that mutations affecting different genes could impact common
186 molecular networks if the respective gene products interact at the molecular level [36]. However,
187 previous analyses were mostly restricted to individual molecular layers. For example, it was shown that
188 genes mutated in different patients often cluster together in molecular interaction networks [36]. Yet,
189 effects of these mutations on transcript and protein levels remained unexplored in this case.

190 Previous work of Sinha and colleagues already suggested extensive *trans*-effects of CNAs on
191 mRNA and protein levels [17]. Thus, here we aimed to systematically explore how different CNA events
192 would impact on the level of one common protein. In order to prioritize potentially interesting proteins
193 for such an analysis, we focused on the 20 proteins with the largest average absolute FCs across all
194 tumor specimens (**Additional file 1: Fig. S8**, **Additional file 7: Table S6**). Thus, these proteins represent a
195 set of proteins that was strongly affected across most tumors independent of tumor grade. Among them
196 was PSA (KLK3), and several other well established PCa-associated proteins like AGR2 [37], MDH2 [38],
197 MFAP4 [39] and FABP5 [40]. RABL3 was one of the most strongly down-regulated proteins, which is a
198 surprising finding as RABL3 is known to be up-regulated in other solid tumors [41, 42]. Interestingly, in
199 most cases these proteins were from loci that were not subject to CNAs (**Additional file 1: Fig. S8**,
200 **Additional file 7: Table S6**), hinting that independent genomic events would impact on these target
201 proteins *via* network effects in *trans*.

202 Among those top targets we selected AGR2, ACPP, POSTN and LGALS3BP for further analysis (**Fig.**
203 **3a**), because these proteins/genes had correlated protein- and mRNA FCs; thus, protein level changes
204 were likely caused by cognate mRNA level changes. To identify potential regulators for each target gene,
205 we used the STRING gene interaction network [43] and selected putative effectors at most one edge
206 away from the target genes. Further, we required that neighbors or the target itself were subject to
207 CNAs in at least four tumor samples ('**Methods**' section). By including the target itself we account for
208 potential CNA *cis*-effects. However, only POSTN passed that filter. This filtering identified 13 neighbors of
209 ACPP, 28 neighbors of POSTN (and POSTN itself), 14 neighbors of LGALS3BP and one neighbor for AGR2,
210 which was not further considered. Next, we correlated CNAs of those neighbor genes with the mRNA FCs
211 of the respective target genes (**Fig. 3b**). We then used the non-neighboring genes (*i.e.* the network
212 complement) to generate a background distribution of CNA-target correlations specifically for each
213 target. Here, we also only considered genes with at least four CNAs across the tumor samples. Since
214 STRING reports predicted functional associations between genes we expected only a minority of the
215 neighbors to actually correlate with their putative targets. Further note that edges in STRING could

216 represent indirect gene-gene relationships. Yet, in the case of ACPP we found that CNA levels of its 13
217 neighbors were on average more strongly correlated with ACPP mRNA FCs than the complement (**Fig.**
218 **3b**). This observation does not preclude the possibility that also some of the POSTN and LGALS3BP
219 neighbors impacted on their mRNA levels in *trans*. However, the fact that ACPP neighbors were on
220 average more strongly correlated with ACPP mRNA FCs, suggested to us that multiple of its network
221 neighbors might be involved in tumorigenic down-regulation of ACPP.

222 ACPP, which is also known as ACP3 or PAcP, is a prostate-specific acid phosphatase with a critical
223 role in PCa etiology and has been suggested as a PCa biomarker long before PSA [44]. ACP3 is known to
224 inhibit cell proliferation and is therefore typically down-regulated in PCa [45], despite elevated ACP3
225 protein levels in patient blood [44]. In our cohort ACP3 levels were strongly down-regulated in all of the
226 high-grade patients and in the vast majority of low- and intermediate-grade patients, suggesting that
227 ACP3 down-regulation represents an early event during PCa evolution. Despite its established role in PCa,
228 little is known about the oncogenic driver events down-regulating ACP3 [44].

229 We speculated that CNA events affecting different ACPP neighbors might be in operation in
230 different tumor specimens. Thus, to further narrow the list of candidates we devised a multi-dimensional
231 regression approach modeling the combined CNA effects of neighbors on ACPP mRNA FCs ('**Methods**'
232 section). Five neighbors (DGUOK, APRT, GOT1L1, NKX3-1 and ENTPD4) had statistically significant effects
233 in that multi-dimensional model (**Fig. 3c**). We utilized two independent PCa cohorts (TCGA; [8] and
234 MSKCC [31]) to validate potential effects of those five genes: we computed the association between the
235 CNAs of each significant regulator and the corresponding mRNA log-FC of ACPP in each cohort and
236 confirmed that the signs of the effects (i.e. effect directions) were the same for all five genes in all
237 cohorts. Among those hits was NKX3-1, which is a prostate-specific tumor suppressor gene and loss of a
238 single allele may predispose to prostate carcinogenesis [46, 47]. NKX3-1 is a transcription factor found to
239 have substantial *trans*-effects in PCa [17]. Consistent with its potential role as an ACPP regulator, NKX3-1
240 has been found to bind within 1 kb of the transcription start site of ACPP ([48]; GEO GSE40269).
241 Interestingly, the CNA signatures of the five putative regulators split into two clusters affecting two
242 distinct sets of patients (**Fig. 3c**): the first one harboring joint deletions of DGUOK and APRT, the second
243 one harboring joint deletions of NKX3-1, ENTPD4 and GOT1L1. The latter three genes are all encoded on
244 Chromosome 8 and thus, their deletion may be due to single CNA events. DGUOK and APRT however,
245 are encoded on different chromosomes. Importantly, these events were clonal in most cases, *i.e.* they
246 were mostly common to both tumor samples of a given patient. Hence, our network analysis hints that
247 distinct deletions in the network vicinity of ACP3 can lead to the repression of this anti-proliferative

248 protein. Taken together, these findings suggest that tumor mechanisms in different patients converged
249 on common protein endpoints.

250 **Joint network effects of CNAs drive tumor progression.**

251 The analysis above identified molecular networks driving tumor alterations and thus indicated
252 altered biochemical states that were common to most tumor specimens. To identify sub-networks that
253 specifically distinguish high-grade from low-grade tumors, we performed a distinct network analysis: we
254 mapped our data onto the STRING gene interaction network [43], and employed network propagation
255 [49, 50] separately to the CNA, transcriptome and proteome data for each of the tumor samples. We
256 excluded point mutations from this analysis as their frequency was too low in our cohort. By combining
257 published molecular interactome data with a network propagation algorithm [36, 49], we aimed to
258 'enrich' network regions with many perturbed genes/proteins. We reasoned that the convergent
259 consequences of genomic variants on common network regions would be indicative of specific
260 biochemical functions that are important for the tumor biology. We therefore identified genes/proteins
261 in network regions that showed a higher score (or a lower score) in high-grade (G4/5) relative to lower-
262 grade (G1) tumor groups at all three levels (Fig. 4a, b; 'Methods' section). This analysis identified sub-
263 networks consisting of over- and under-expressed genes (relative to the benign controls). We found 57
264 amplified genes (Additional file 7: Table S6) for which transcripts and proteins were often over-
265 expressed in high-grade PCa (Fig. 4a) and 21 genes with copy number loss (Additional file 7: Table S6)
266 for which transcripts and proteins were often down-regulated compared to lower-grade tumors (Fig. 4b).

267 Among the up-regulated network nodes, we observed genes modulating the stability of
268 chromatin, such as chromatin-binding protein Chromobox 1 (CBX1) [51], SET Domain Bifurcated 1
269 (SETDB1) [52], a function linking to H3K27me3 and H3K9me3 in chromatin, and CBX3 (known as HP1-γ)
270 [53]. SETDB1 is an oncogene in melanoma [54] and has also been found to be over-expressed in PCa and
271 cell lines [55]. Further, we found genes involved in DNA damage repair, such as SMG7 [56] and ATR [57],
272 and PRKCZ [58], which had already been suggested as a biomarker prognostic for survival in PCa [59].
273 Multiple actin related proteins including ARPC1B [60], ARPC5 [61], ACTL6A [62], and CFL1 [63], which are
274 markers for aggressive cancers, were part of the up-regulated network nodes. Moreover, the up-
275 regulated genes contained proteins related to the cell cycle like BANF1 and proteins interacting with the
276 centrosome including LAMTOR1 and RAB7A that had already been associated with PCa [64]. Finally,
277 several signaling molecules with known roles in PCa were up-regulated, such as the transcription factor
278 Yin Yang 1 (YY1) [65], the TGF-β receptor TGFBR1 [66], and KPNA4, which promotes metastasis through

279 activation of NF- κ B and Notch signaling [67]. Thus, up-regulated network nodes are involved in
280 DNA/chromatin integrity and growth control.

281 Likewise, several of the down-regulated genes had functions associated with PCa. For example,
282 the oxidative stress related gene MGST1, which is recurrently deleted in PCa [68]. ALDH1A3 is a direct
283 androgen-responsive gene, which encodes NAD-dependent aldehyde dehydrogenase [69]. DHCR24 is
284 involved in cholesterol biosynthesis and regulated by the androgen receptor [70]. Polymorphisms in
285 CYP1A1 are associated with PCa risk in several meta-analyses among different ethnicities [71-73].

286 Further, our network analysis is suggesting tumor mechanisms converging on genes that are
287 known contributors to PCa tumor biology. For example, the PCa-associated gene SF3B2 [74, 75] was only
288 weakly amplified in some of the high-grade tumors (average $\log_2FC = 0.016$) and mRNA levels showed
289 similarly small changes (average $\log_2FC = 0.024$). On the other hand, the SF3B2 protein levels were
290 consistently and more strongly up-regulated across tumors (average $\log_2FC = 0.31$), especially within the
291 high-grade tumors (**Additional file 1: Fig. S9**). Another example is UBE2T whose over-expression is
292 known to be associated with PCa [76]. Unfortunately, we could not quantify the corresponding protein
293 levels. However, we observed a strong and consistent mRNA over-expression across several tumors
294 (average $\log_2FC = 0.73$), even though at the DNA level the gene was only weakly amplified (average
295 $\log_2FC = 0.023$; **Additional file 1: Fig. S9**). Our findings of more heterogeneous CNAs, but more uniform
296 mRNA and protein alterations point on convergent evolutionary mechanisms, as we move along the axis
297 of gene expression.

298 Next, we analyzed the largest connected component with genes up-regulated in advanced
299 disease in more detail (see the '**Methods**' section). It consists of the nine nodes EMD, BANF1, ACTL6A,
300 YY1, RUVBL1, KANSL1, MRGBP, VPS72 and ZNHIT1 (**Fig. 4a**), and is referred to in the following as
301 Network Component 1 (**Additional file 7: Table S6**). Seven of these proteins are involved in chromosome
302 organization which may induce genomic alterations and influence the outcome of multiple cancers
303 including PCa [77]. For example, the actin-related protein ACTL6A is a member of the SWI/SNF (BAF)
304 chromatin remodeling complex [78], and a known oncogene and a prognostic biomarker for PCa [79].
305 Further, ACTL6A, RUVBL1 and MRGBP are together part of the NuA4/Tip60-HAT complex, which is
306 another chromatin remodeling complex involved in DNA repair [80]. Likewise, KANSL1 is involved in
307 histone post-translation modifications, while VPS72 is a member of histone- and chromatin remodeling
308 complexes [81]. Thus, Network Component 1 consists of genes involved in chromatin remodeling and
309 DNA repair, many of which are known to be involved in cancers.

310 Several samples were characterized by a small, but consistent DNA amplification of multiple
311 members of Network Component 1 (**Fig. 4c**). Out of the 66 tumor samples, there were 30 samples –
312 belonging to all grade groups – with a weak but remarkably consistent DNA amplification of Network
313 Component 1 members, while the high-grade samples had stronger amplifications on average (i.e. larger
314 effect sizes). Importantly, gene members of Network Component 1 were dispersed across eight
315 chromosomes (**Additional file 7: Table S6**). The parallel DNA amplification of these genes is therefore
316 the result of multiple independent CNA events, while the signal on any single gene alone was too weak
317 to be significant in isolation. Further, members of Network Component 1 were consistently amplified in
318 both tumor areas (i.e. TA1 and TA2) of six patients (H2, H4, H5, H6, H8, and H9; **Fig. 4c**), thus establishing
319 them as likely clonal events. In some but not all cases, the amplifications led to a small, but consistent
320 increase in mRNA expression of the amplified gene loci (**Fig. 4c**). We were able to reconcile 40 tumor
321 samples with a significant enrichment of this network component in either the CNA or mRNA layer.
322 Unfortunately, only three out of the nine proteins were detected in our proteomics experiments (**Fig. 4c**).
323 Interestingly, patients where the DNA amplifications led to transcript over-expression were almost
324 always high-grade patients, whereas patients where the amplification affected gene expression to a
325 smaller extent were low- or intermediate-grade patients (**Fig. 4c**). Further, we noticed that TA2 samples
326 graded as G3 from high-grade patients carried amplifications of Network Component 1, whereas tumor
327 areas graded as G3 from intermediate-grade patients did not have amplifications of this network
328 component (**Fig. 4c**). Thus, although the tumor areas were histologically equally classified, tumor areas
329 from high-grade patients carried a CNA signature and expression patterns reminiscent of the high-grade
330 areas from the same patients. Therefore, within the cohort tested the joint DNA amplification of this
331 network component along with RNA up-regulation is a signature of high-grade tumors. Curiously, the
332 higher-grade tumor areas of those high-grade patients (TA1) carried stronger DNA amplifications than
333 the respective lower-grade areas (TA2), which implies that the progressive amplification of Network
334 Component 1 during tumor evolution may contribute to an increasingly aggressive phenotype. To
335 further corroborate the clinical relevance of this network perturbation, we analyzed published datasets
336 of three additional PCa cohorts (TCGA[8], MSKCC [31], and Aarhus [82]), together comprising a total of
337 709 patients with known clinical outcome. We found that amplification of genes from Network
338 Component 1 was a significant predictor of reduced RFS in the MSKCC cohort (P value = 8.8e-3, log-rank
339 test). In the TCGA cohort, we observed the same trend although the difference in RFS was not
340 statistically significant (P value = 0.17; **Fig. 4d**). Additionally, we found that over-expression of genes
341 from Network Component 1 was a significant predictor of reduced RFS in the TCGA cohort (P value =

342 2.1e-4, log-rank test), which was the cohort with the largest number of patients. In the other two
343 cohorts we observed the same trend, although the difference in RFS was not statistically significant (P
344 value = 0.30 and 0.093 for MSKCC, and Aarhus; **Fig. 4d**). Thus, both CNA and RNA changes of Network
345 Component 1 are predictive of the time to relapse in independent cohorts. To also account for
346 covariates, we fitted Cox proportional-hazards models with the age and the copy number burden as
347 (additional) covariates. When including only the age in our model, the results showed minor changes
348 (**Fig. 4d**). When including both the age and the copy number burden in our model, the effect direction of
349 Network Component 1 remained the same but was not statistically significant anymore (P value = 0.055
350 for TCGA, mRNA and P value = 0.064 for MSKCC, CNA).

351 In conclusion, our findings suggest that relatively weak but broad CNAs of entire network
352 components are associated with high-grade tumors and that the presence of some of these
353 perturbations in lower-grade tumors may be predictive of the future development of a more aggressive
354 phenotype.

355 **Analysis of distinct tumor nodules defines intra-patient heterogeneity (TA1 versus
356 TA2 comparison).**

357 The CNA patterns (**Additional file 1: Fig. S4**) and the Network Component 1 analysis (**Fig. 4c**)
358 suggest that different tumor areas from the same patient shared several mutations. Such common
359 signatures are expected if different tumor nodules originate from a common clone. If this was true, we
360 would expect mutational signatures to be more similar between different nodules from the same patient
361 than between patients, even though mutated genes may be shared across patients. To compare the
362 intra- and inter-patient molecular heterogeneity at the levels of CNAs, transcript, and protein FCs, we
363 computed the Pearson correlation between tumor area 1 (TA1) and its paired tumor area 2 (TA2) for
364 each layer and all of the 27 patients with two characterized tumor areas (25 for the mRNA, see the
365 ‘Methods’ section and **Additional file 1: Supplementary Text**). As a control, we also computed all
366 pairwise Pearson correlations between the samples within each of the grade groups (*i.e.* inter-patient
367 correlation). As expected, paired TA1 and TA2 from the same patient were on average more strongly
368 correlated to each other compared to samples from different patients within the same grade group. This
369 finding was consistent for all omics layers (**Fig. 5a**), and was more pronounced at the CNA and mRNA
370 layers compared to the protein layer.

371 Next, we tested whether a high correlation at the level of CNAs also implies a high correlation at
372 the level of mRNA and proteins. We tested this idea by ‘correlating the correlations’, *i.e.* we correlated

373 the TA1-TA2 correlation of CNA profiles with the correlation between the mRNA and protein profiles of
374 the same tumor areas (**Fig. 5b**). Indeed, a higher correlation of two tumor areas at the level of CNA
375 correlated significantly with a higher correlation at the level of mRNA ($r=0.49$, P value=0.014). In other
376 words, knowing how similar two tumor areas of a patient are at the CNA level supports a prediction of
377 their similarity at the mRNA level (and conversely). Although the correlation between protein and CNA
378 was not statistically significant, it followed the same trend ($r=0.35$, P value=0.076).

379 Comparing molecular similarity across omics layers allowed us to identify specific types of
380 patients. The patients H2, H4, M13 had highly correlated tumor areas at all three layers (upper right
381 corner in all scatterplots of **Fig. 5b**). Likely, the tumor areas of these patients have a common clonal
382 origin (**Additional file 1: Fig. S3**). In contrast, patients M12 and M14 had weakly correlated tumor areas
383 at all levels (bottom left corner in all scatterplots of **Fig. 5b**). These tumor nodules either have
384 independent clonal origins or they diverged at an earlier stage during tumor evolution (**Additional file 1:**
385 **Fig. S3**) [16]. For example, in the case of patient M12 large parts of the genome were not affected by
386 CNAs in the benign sample as well as in TA1 and TA2. However, as shown on **Additional file 1: Fig. S3**, a
387 large region was amplified in TA1, whereas the same region was deleted in TA2. This is consistent with a
388 scenario in which TA1 and TA2 show parallel evolution. A third class of patients is exemplified by the
389 patients M9 and M17, who showed a high correlation between their tumor areas on the CNA and mRNA
390 levels, but not on the protein level. Yet other patterns were apparent in patients M4, M7, and H10. They
391 showed similar mRNA and protein patterns in the two tumor areas, but relatively uncorrelated CNAs.
392 The results here apply to global proteome patterns and therefore hint that such convergent network
393 effects of CNAs can be frequent. We confirmed that protein-level similarity correlated with similar
394 histological characteristics of the tumor areas. **Additional file 1: Fig. S10** shows formalin-fixed paraffin-
395 embedded (FFPE) tissue microarray images (duplicates) from the analyzed tumor nodules (TA1 and TA2,
396 diameter 0.6 mm), further underlining the hypothesis that ultimately protein-level alterations are
397 responsible for common cellular phenotypes. Although we cannot fully exclude the possibility that some
398 of these results were affected by technical noise in the data, our findings suggest that transcript
399 alterations can frequently be buffered at the level of proteins (patients M9, M17, **Additional file 1: Fig.**
400 **S7**) and that convergent evolutionary processes may lead to the alteration of common proteins (patients
401 M4, M7, H10). We also note that our findings are specific to the two tumor areas available in this study
402 and could be different if other nodules had been sampled for each of the patients. However, our findings
403 on patients with weakly correlated tumor areas at all levels like M12 and M14 suggest that these
404 patients might carry more than one disease [16].

405 Discussion

406 Despite twenty years of oncological research involving genome-scale (omics) technologies, we
407 know remarkably little about how the discovered genomic alterations affect the biochemical state of a
408 cell and consequently the disease phenotype. In particular, little is known about how genomic
409 alterations propagate along the axis of gene expression [17, 18]. Here, we have exploited recent
410 technological advances in data acquisition that made it possible to characterize small samples of the
411 same tumor specimens at the level of genomes, transcriptomes, and proteomes and advances in
412 computational strategies towards the network-based integration of multi-omics data.

413 In our study, samples were generated from small, less than 1 mm diameter punches in
414 immediate spatial proximity in the tumor and subsequently profiled at all three 'omics layers' (DNA, RNA,
415 proteome). Due to the large spatial heterogeneity of PCa [14, 24], this design - which is so far uncommon
416 for studies profiling multiple layers from tumor specimens - was instrumental for increasing the
417 comparability of the various omics layers and thus facilitated the analysis of molecular mechanisms. Our
418 key findings are: (1) we confirmed the importance of CNAs for PCa biology and the alteration of many
419 known PCa-associated genes at the transcript- and protein-level; (2) we revealed a generally elevated
420 molecular alteration of high-grade tumors compared to lower-grade tumors; (3) although our study
421 confirmed large within- and between-patient genomic heterogeneity, (4) we detected molecular
422 networks that were commonly altered at the mRNA and protein-level. The fact that many of those target
423 molecules are known drivers of PCa tumorigenesis, supports the notion that these proteins/transcripts
424 are subject to convergent evolutionary mechanisms.

425 We integrated the three omics layers using a network-based approach as opposed to directly
426 comparing gene perturbations (mutations) to gene products (transcripts and proteins). Using genome
427 data only, it had previously been hypothesized that whereas the identity of specific mutated genes may
428 differ between tumors, those mutations might still affect common molecular networks [36]. In other
429 words, tumor phenotypes are determined by the perturbation of molecular networks and not by the
430 perturbation of isolated genes. Our study provides experimental evidence that such network effects are
431 indeed propagated to subsequent molecular layers and that this effect propagation may be clinically
432 relevant. A very prominent example is the indication derived from our data that the long-known PCa
433 gene ACPP (ACP3) is downregulated through diverse CNA events. Of particular interest is the potential
434 role of NKX3-1 in ACP3 downregulation. Although both genes have a well-established PCa association
435 their regulatory relationship had not been reported so far (to our knowledge).

436 Our multi-omics network analysis revealed molecular sub-networks that distinguished high-
437 grade PCa tumors from low-grade tumors. Specifically, our analysis led to the identification of Network
438 Component 1, a sub-network involved in chromatin remodeling and consisting of genes that were
439 weakly amplified in intermediate-grade (G3) tumor specimens. Signals of individual gene members of
440 this component were virtually indistinguishable from noise in our cohort. However, their consistent
441 alterations across the network region, across molecular layers and the fact that the same genes showed
442 enhanced signals in high-grade specimens, rendered this component highly interesting. The fact that
443 copy number and expression changes of Network Component 1 members were predictive for survival in
444 independent cohorts further supports the potential clinical relevance of this sub-network. Amplification
445 of Network Component 1 was to some extent confounded with overall CNA burden ($r=0.58$ (TCGA, CNA),
446 $r=0.55$ (TCGA, mRNA), $r=0.34$ (MSKCC, CNA), $r=0.16$ (MSKCC, mRNA)). However, the amplifications of
447 Network Component 1 members were highly correlated and on average above the background of CNAs.
448 Thus, the coordinated amplification of Network Component 1 does not simply mirror overall CNA burden.
449 Our network-based cross-omics analysis identified nine other network components (Fig. 4) successfully
450 capturing several known and potentially new PCa-associated genes. However, neither Network
451 Component 1 nor any of the other network components was uniformly subject to CNAs across all high-
452 grade patients. Instead, we found different network components modified in different patients and
453 these sub-networks were involved in cellular processes as diverse as actin remodeling, DNA damage
454 response, and metabolic functions, all of which are known contributors to PCa biology. This further
455 underlines the large inter-patient variability of PCa and it demonstrates the diversity of molecular
456 mechanisms leading to histologically similar phenotypes. Future prediction models of PCa including the
457 ISUP grade groups, PSA levels and clinical stage might be improved by exploiting multi-omics network
458 analyses. Detecting aggressive networks alterations in prostate biopsies would help clinicians to advice
459 either active surveillance or active therapy. However, the development of such multi-dimensional
460 biomarkers would require much larger patient cohorts.

461 Another distinguishing feature of this study was the simultaneous profiling of two different
462 tumor regions in 27 out of the 39 patients. The profiling of multiple tumor regions from the same
463 prostate helped to further highlight the enormous heterogeneity of PCa within patients and provided
464 important insights into PCa evolution. The fact that Network Component 1 was more strongly affected in
465 the paired higher-grade nodules of high-grade patients suggests that at least certain sub-networks are
466 subject to an evolutionary process, that progressively 'moves' protein levels towards a more aggressive
467 state. Generally, and at all molecular layers tested, the two paired tumor areas were more similar to

468 each other compared to two samples from the same grade group but different patients, suggesting
469 common evolutionary origins. Although the two tumor areas seemed to mostly originate from the same
470 clone, this was not always the case. In some patients, different nodules exhibited different molecular
471 patterns at all omics layers, suggesting early evolutionary separation. Thus, for the first time, current
472 diagnostic, expert-level consensus guidelines [28] are supported by detailed proteogenomic data. Our
473 findings support earlier claims that clonality itself might be a prognostic marker with implications for
474 future, more tumor-specific treatment when targeted therapies become available also for PCa [16, 83].

475 Our study shows that all three molecular layers (genome, transcriptome and proteome)
476 contributed valuable information for understanding the biology of PCa. In particular the DNA layer
477 informed about causal events, clonality, and genomic similarity between tumors. The transcriptome was
478 relevant for understanding the transmission of CNA effects to proteins and served as a surrogate in cases
479 where protein levels remained undetected. The proteome was crucial for revealing protein-level
480 buffering of CNA effects as well as for indicating convergent evolution on functional endpoints. In a
481 routine diagnostic context though, measuring all three layers may not be feasible for the near future due
482 to resource and time limitations. Thus, the identification of improved, routine-usable molecular markers
483 for PCa diagnostics and prognosis remains an open problem [17].

484 **Conclusions**

485 This study uncovered molecular networks with remarkably convergent alterations across tumor
486 sites and patients. In particular, we identified a sub-network consisting of nine genes whose joint activity
487 positively correlated with increasingly aggressive tumor phenotypes. The fact that this sub-network was
488 predictive for survival in independent cohorts further supports its potential clinical relevance. At the
489 same time though, our study also exposed a diversity of network effects: we could not identify a single
490 sub-network that was perturbed in all high-grade tumor regions, let alone the observed distinct intra-
491 patient alterations at all omics layers for some patients. Overall, our study has significantly expanded our
492 understanding of PCa biology and serves as a model for future work aiming to explore network effects of
493 mutations with an integrated multi-omics approach.

494

495 Methods

496 Patients and samples

497 A total of 39 men with localized PCa who were scheduled for RP were selected from a cohort of
498 1,200 patients within the ProCOC study and processed at the Department of Pathology and Molecular
499 Pathology, University Hospital Zurich, Switzerland [25]. Each of the selected intermediate- and high-
500 grade patients had two different tumor nodules with different ISUP grade groups. H&E (Hematoxylin and
501 Eosin)-stained fresh frozen tissue sections of 105 selected BPH and tumor regions were evaluated by two
502 experienced pathologists (PJW, NJR) to assign malignancy, tumor stage, and Grade Group according to
503 the International Union Against Cancer (UICC) and WHO/ISUP criteria. This study was approved by the
504 Cantonal Ethics Committee of Zurich (KEK-ZH-No. 2008-0040), the associated methods were carried out
505 in accordance with the approved guidelines, and each patient has signed an informed consent form.
506 Patients were followed up on a regular basis (every three months in the first year and at least annually
507 thereafter) or on an individual basis depending on the disease course in the following years. The RFS was
508 calculated with a biochemical recurrence (BCR) defined as a PSA ≥ 0.1 ng/ml. Patients were censored if
509 lost to follow-up or event-free at their most recent clinic visit. Patients with a postoperative PSA
510 persistence or without distinct follow-up data for the endpoint BCR were excluded from the analysis of
511 BCR.

512 Exome sequencing and somatic variant analysis

513 The exome sequencing (exome-seq) was performed using the Agilent Sure Select Exome
514 platform for library construction and Illumina HiSeq 2500 for sequencing read generation. We mapped
515 and processed the reads using a pipeline based on bowtie2 [84] (1.1.1) and the Genome Analysis Tools
516 Kit (GATK) [85] (3.2-2). We detected and reported nonsynonymous variants or variants causing splicing
517 changes using Strelka (1.0.14) and Mutect (1.1.7) combined with post-processing by the CLC Genomics
518 Workbench (8.0.3). In this process, all tissue samples of a patient were compared to the respective blood
519 sample.

520 Trimmomatic [86] (0.36) was used for adaptor clipping and low-quality subsequence trimming of
521 the FASTQ files. Subsequently, single reads were aligned to the hg19 reference genome with bowtie2
522 with options “--very-sensitive -k 20”. We applied samtools [87] (0.1.19) and picard-tools (1.119) to sort
523 the resulting bam files in coordinate order, merge different lanes, filter out all non-primary alignments,

524 and remove PCR duplicates. Quality of the runs was checked using a combination of BEDtools [88] (2.21),
525 samtools, R (3.1) and FastQC (0.11.2).

526 Bam files containing the mapped reads were preprocessed in the following way: indel
527 information was used to realign individual reads using the RealignerTargetCreator and IndelRealigner
528 option of the GATK. Mate-pair information between mates was verified and fixed using Picard tools and
529 single bases were recalibrated using GATK's BaseRecalibrator. After preprocessing, variant calling was
530 carried out by comparing benign or tumor prostate tissue samples with matched blood samples using
531 the programs MuTect [89] and Strelka [90] independently. Somatic variants that were only detected by
532 one of the two programs were filtered out using CLC Genomics Workbench. So were those that had an
533 entry in the dbSNP [91] common database and those that represented synonymous variants without
534 predicted effects on splicing.

535 **CNA analysis of exome-seq data**

536 The Bam files generated during the process of somatic variant calling were processed with the
537 CopywriteR package (v.2.2.0) for the R software [92]. CopywriteR makes use of so-called "off-target"
538 reads, *i.e.* reads that cover areas outside of the exon amplicons. "Off-target" reads are produced due to
539 inefficient enrichment strategies. In our case on average 28.5% of the total reads were not on target.
540 Briefly, CopywriteR removes low quality and anomalous read pairs, then peaks are called in the
541 respective blood reference, and all reads in this region are discarded. After mapping the reads into bins,
542 those peak regions, in which reads had been removed, were compensated for. Additionally, read counts
543 are corrected based on mappability and GC-content. Finally, a circular binary segmentation is carried out
544 and for each segment the log count ratios between tissue samples and the respective blood sample are
545 reported as copy number gain or loss. The copy number of each gene in each sample was reported
546 based on the log count ratio of the respective segment in which the gene was located. The overall
547 performance of this CNA-calling approach was evaluated by comparing the results of the TA1 (and TA)
548 samples with CNA results obtained by applying the OncoScan Microarray pipeline to FFPE samples from
549 the same tumors (**Additional file 1: Fig. S11**).

550 **OncoScan Microarrays**

551 OncoScan copy number assays were carried out and analyzed as described previously [93].
552 Briefly, DNA was extracted from punches of FFPE cancer tissue blocks. Locus-specific molecular inversion
553 probes were hybridized to complementary DNA and gaps were filled in a nucleotide-specific manner.

554 After amplification and cleavage of the probes, the probes were hybridized to the OncoScan assay
555 arrays. Scanning the fluorescence intensity and subsequent data processing using the Affymetrix®
556 GeneChip® Command Console and BioDiscovery Nexus express resulted in log intensity ratio data
557 (sample versus Affymetrix reference) and virtual segmentation of the genome into areas with copy
558 number gain, loss or stability.

559 RNA Sequencing

560 RNA sequencing was performed at the Functional Genomics Center Zurich. RNA-seq libraries
561 were generated using the TruSeq RNA stranded kit with PolyA enrichment (Illumina, San Diego, CA, USA).
562 Libraries were sequenced with 2x126bp paired-end on an Illumina HiSeq 2500 with an average of 105.2
563 mio reads per sample.

564 Paired-end reads were mapped to the human reference genome (GRCh37) using the STAR
565 aligner (version 2.4.2a) [94]. Quality control of the resulting bam files using QoRTs [95] and mRIN [96]
566 showed strong RNA degradation[97] in a significant fraction of the samples: mRIN classified 31 samples
567 as highly degraded (**Additional file 1: Fig. S12, Additional file 5: Table S4**). In order to correct for this 3'
568 bias, 3 tag counting was performed as described by Sigurgeirsson et al [98] using a tag length of 1,000.
569 After 3' bias correction, three samples still showed a clear 3' bias: the two tumor regions (TA1 and TA2)
570 of the patient M5 and TA2 from patient M8 (**Additional file 1: Fig. S12**). These samples were excluded
571 from subsequent analyses. Additionally, the BPH region of the patient M5 was excluded due to the
572 exclusion of both its tumor regions.

573 FeatureCounts [99] was used to determine read counts for all genes annotated in ENSEMBL v75.
574 Genes for which no read was observed in any of the samples in the original data were excluded from the
575 analysis. Further, after 3 tag counting, all genes with without at least 1 read per million in N of the
576 samples were removed. We chose N to be 10 which corresponds to the size of the smallest grade group
577 (G2). In a last reduction step, all genes with more than one transcript were excluded, yielding a final set
578 of 14,281 genes.

579 Read count normalization and differential gene expression analysis was performed using the R
580 packages sva [100] and DESeq2 [101]. All benign tissues were considered biological replicates and
581 differential gene expression for the individual tumor samples was determined against all benign tissues.
582 Gene expression changes with an adjusted *P* value < 0.1 were considered significant.

583 **RNA-seq - 3' bias correction**

584 The 3 tag counting approach for 3' bias correction was used on the RNA-seq dataset [98]. This
585 approach requires changing of the annotation file in two steps: 1) isoform filtering and 2) transcript
586 length restriction. As proposed in [98] for each gene we determined the highest expressed isoform
587 within a set of high quality samples. As high quality samples we used all samples with an mRIN score
588 greater than or equal to 0.02. This set contains 7 benign and 15 tumor samples. Isoform expression was
589 determined using cufflinks [102]. As transcript length we chose 1,000bp.

590 **Gene fusions**

591 FusionCatcher (version 0.99.5a beta) was used to determine gene fusions for all samples.
592 Fusions classified as “probably false positive” are discarded unless they are also classified as “known
593 fusion”.

594 **PCT assisted sample preparation for SWATH-MS**

595 We first washed each tissue sample to remove O.C.T., followed by PCT-assisted tissue lysis and
596 protein digestion, and SWATH-MS analysis, as described previously [23]. Briefly, a series of ethanol
597 solutions were used to wash the tissues each tissue, including 70% ethanol / 30% water (30 s), water (30
598 s), 70% ethanol / 30% water (5 min, twice), 85% ethanol / 15% water (5 min, twice), and 100% ethanol (5
599 min, twice). Subsequently, the tissue punches were lysed in PCT-MicroTubes with PCT-MicroPestle [103]
600 with 30 μ l lysis buffer containing 8 M urea, 0.1 M ammonium bicarbonate, Complete protease inhibitor
601 cocktail (Roche) and PhosSTOP phosphatase inhibitor cocktail (Roche) using a barocycler (model
602 NEP2320-45k, PressureBioSciences, South Easton, MA). The lysis was performed with 60 cycles of high
603 pressure (45,000 p.s.i., 50 s per cycle) and ambient pressure (14.7 p.s.i., 10 s per cycle). The extracted
604 proteins were then reduced and alkylated prior to lys-C and trypsin-mediated proteolysis under pressure
605 cycling. Lys-C (Wako; enzyme-to-substrate ratio, 1:40) -mediated proteolysis was performed using 45
606 cycles of pressure alternation (20,000 p.s.i. for 50 s per cycle and 14.7 p.s.i. for 10 s per cycle), followed
607 by trypsin (Promega; enzyme-to-substrate ratio, 1:20)-mediated proteolysis using the same cycling
608 scheme for 90 cycles. The resultant peptides were cleaned using SEP-PAC C18 (Waters Corp., Milford,
609 MA) and analyzed, after spike-in 10% iRT peptides ⁵¹, using SWATH-MS following the 32-fixed-size-
610 window scheme as described previously ^{19, 21} using a 5600 TripleTOF mass spectrometer (Sciex) and a
611 1D+ Nano LC system (Eksigent, Dublin, CA). The LC gradient was formulated with buffer A (2%
612 acetonitrile and 0.1% formic acid in HPLC water) and buffer B (2% water and 0.1% formic acid in

613 acetonitrile) through an analytical column (75 μ m \times 20 cm) and a fused silica PicoTip emitter (New
614 Objective, Woburn, MA, USA) with 3- μ m 200 \AA Magic C18 AQ resin (Michrom BioResources, Auburn, CA,
615 USA). Peptide samples were separated with a linear gradient of 2% to 35% buffer B over 120 min at a
616 flow rate of 0.3 μ l min $^{-1}$. Ion accumulation time for MS1 and MS2 was set at 100 ms, leading to a total
617 cycle time of 3.3 s.

618 **SWATH assay query library for prostate tissue proteome**

619 To build a comprehensive library for SWATH data analysis, we analyzed unfractionated prostate
620 tissue digests prepared by the PCT method using Data Dependent Acquisition (DDA) mode in a tripleTOF
621 mass spectrometer over a gradient of 2 hours as described previously¹⁹. We spiked iRT peptides⁵¹ into
622 each sample to enable retention time calibration among different samples. We then combined these
623 data with the DDA files from the pan-human library project [104]. All together we analyzed 422 DDA files
624 using X!Tandem⁵² and OMSSA⁵³ against three protein sequence databases downloaded on Oct 21, 2016
625 from UniProt, including the SwissProt database of curated protein sequences (n=20,160), the splicing
626 variant database (n=21,970), and the trembl database (n=135,369). Using each database, we built target-
627 decoy protein sequence database by reversing the target protein sequences. We allowed maximal two
628 missed cleavages for fully tryptic peptides, and 50 p.p.m. for peptide precursor mass error, and 0.1 Da
629 for peptide fragment mass error. Static modification included carbamidomethyl at cysteine, while
630 variable modification included oxidation at methionine. Search results from X!Tandem and OMSSA were
631 further analyzed through Trans-Proteomic Pipeline (TPP, version 4.6.0)⁵⁴ using PeptideProphet and
632 iProphet, followed by SWATH assay library building procedures as detailed previously^{19, 55}. Altogether,
633 we identified 167,402 peptide precursors, from which we selected the proteins detected in prostate
634 tissue samples, and built a sample-specific library. SWATH wiff files were converted into mzXML files
635 using ProteoWizard⁵⁶ msconvert v.3.0.3316, and then mzML files using OpenMS⁵⁷ tool FileConverter.
636 OpenSWATH[105] was performed using the tool OpenSWATHWorkflow with input files including the
637 mzXML file, the TraML library file, and TraML file for iRT peptides.

638 **Peptide quantification using OpenSWATH**

639 To obtain consistent quantification of the SWATH files, we obtained the all annotated *b* and *y*
640 fragments from the sp, sv and tr libraries. About ten thousand redundant and low-quality assays were
641 removed. Then we extracted the chromatography of these fragments and MS1 signals using
642 OpenSWATHWorkflow, followed by curation using DIA-expert[106]. Briefly, the chromatography of all

643 fragments and MS1 signals were subject to scrutiny by empirically developed expert rules. A reference
644 sample with best q value by pyprophet was picked up to refined fragments. The peptide precursors are
645 further filtered based on the following criteria: i) remove peptide precursors with a q value higher than
646 1.7783e-06 to achieve a false discovery rate of 0.00977 at peptide level using SWATH2stats [107]; ii)
647 peptides with a FC higher than 2 between the reference sample and its technical replicate were
648 removed; iii) peptides matching to multiple SwissProt protein sequences were removed. The data matrix
649 was first quantile normalized, \log_2 transformed, followed by batch correction using the ComBat R
650 package [108]. Finally, for each protein and pair of technical replicates the average value was computed.

651 **Statistical analysis**

652 All plots were produced with R. Kaplan-Meier estimators were used for RFS analysis. Differences
653 between survival estimates were evaluated by the log-rank test.

654 **Computation of molecular perturbation scores**

655 On the genomic level (mutation and CNA), we kept the tumor samples (66 in total) that contain
656 FCs with respect to the blood. The mutation matrix was further discretized by setting all non-zero events
657 to 1. At the transcriptomics level, the FCs for the 63 tumor samples were computed as described above
658 (see 'RNA Sequencing'). Finally, on the proteomics level, we computed the FCs for the tumor samples (66
659 in total) as follows: for each protein, its mean intensity over the normal samples was subtracted from
660 the intensities of the tumor samples. (We chose to compute the FCs for the tumor samples with respect
661 to a global reference (average of all normal samples) and not with respect to their paired benign sample
662 in order to achieve a higher consistency with the transcriptomics level.)

663 We assigned to each sample two molecular perturbation scores summarizing/quantifying the
664 magnitude of its FCs: DE_count counts the number of mutated/differentially expressed (DE) genes, while
665 the DE_sum score is the sum of absolute FCs of all genes. Thus, while the first score counts the number
666 of events (mutations/DE genes), the second one quantifies their magnitude. These two scores can be
667 regarded as generalizations of the term 'mutational burden' for the mRNA and protein layer. A gene is
668 regarded as mutated/DE if its value is 1 in the mutation layer and if its absolute value is above a
669 threshold that has been set to 1 for the mRNA and protein layer. For the CNA layer, the corresponding
670 threshold was set to 0.5 because the range of FCs in the CNA matrix is smaller than the mRNA and
671 protein matrices. Both types of scores were computed for each molecular level, except for the point
672 mutations where only DE_count was computed. Afterwards, the 66 DE_count scores (63 for the mRNA)

673 and the DE_sum scores at each layer were divided into the four grade groups G1, G2, G3 and G4/5
674 respectively.

675 **Correlating CNAs with mRNA and protein layer**

676 For each of the 2,120 genes measured in all three layers (CNA, mRNA and protein), we computed
677 the Spearman correlation between its CNAs and corresponding mRNA FCs as well as between its CNAs
678 and corresponding protein FCs. We reduced each layer to the 63 tumor samples with available mRNA
679 data.

680 **Network propagation/smoothing**

681 As a network, the STRING gene interaction network (version 10)[43] was used, after removing all
682 edges with combined score smaller or equal to 0.9 and keeping subsequently the largest connected
683 component. The resulting network consisted of 10,729 nodes and 118,647 (high-confidence) edges. For
684 the network smoothing, the weight matrix was computed as described in Vanunu et al.[49], but for an
685 unweighted graph and the propagation parameter was set to 0.5. The propagation was iteratively
686 repeated 500 times to ensure convergence of the results. For the mapping from gene symbols to STRING
687 identifiers (**Additional file 7: Table S6**) we used the R/Bioconductor package STRINGdb [109]. The gene
688 symbols with no matching STRING identifier were removed, while for those that mapped to multiple
689 STRING identifiers, the first mapping was kept (default choice in the package). From the multiple gene
690 symbols that mapped to the same STRING identifier, the first mapping was kept. The genes that were
691 not present in the network were removed from the datasets, while those that were present in the
692 network but not in the corresponding dataset were initially filled in with 0's.

693 Genes with very small, 'smoothed' (absolute) FCs were filtered out as follows: after the network
694 propagation, only network nodes that had protein measurements themselves or at least one direct
695 neighbor (on the filtered STRING network) with protein measurements were considered in the next
696 steps of this analysis. *I.e.* network nodes without measured FCs at the protein layer that had no direct
697 neighbor with measured protein values were removed from the subsequent analyses.

698 For significance testing, the one-sided Wilcoxon rank sum test comparing the smoothed FCs
699 between the groups G4/5 (consisting of 12 samples for the CNA, mRNA and protein layer) and G1
700 (consisting of 26 samples for the CNA and proteins and 25 for the mRNA) was applied to each network
701 node (after filtering) and layer, once for up-regulation and once for down-regulation. The resulting sub-

702 networks (up-regulated and down-regulated) consisted of those genes that were significant (*P* value
703 below 0.05) at all three layers and all of the edges connecting them on the filtered STRING network.

704 It should be noted that although measurements from the same patient might not be statistically
705 independent, we have kept them in our analyses firstly in order to increase statistical power and
706 secondly because not all of them correspond to clonal events as shown on **Fig. 5**. To make sure though
707 that having two samples for some of the patients has not affected our conclusions, we have repeated
708 the statistical testing step (one-sided Wilcoxon rank sum test) in two ways: comparing G4/5 with G1 as
709 before but removing the second tumor area of a patient if it belonged to the same grade group as tumor
710 area 1 (*i.e.* removing TA2 of patients H3 and H10), and secondly comparing G4/5 with the combined (G1
711 and G2) group and once again removing the second tumor area of a patient if it belonged to the same
712 grade group as his tumor area 1. *P* values resulting from these analyses were highly correlated
713 (**Additional file 1: Fig. S9**), and we would thus consider the current conclusions to be robust.

714 **Network Component 1 analysis**

715 For each tumor sample at the CNA layer, a one-sided, one-sample t-test has been applied testing
716 if its average FC over the genes of the Network Component 1 (and in particular those that have been
717 measured at the CNA) is significantly greater than 0. Due to the presence of outliers in some samples,
718 the non-parametric, one-sided Wilcoxon signed-rank test has been applied as well yielding very similar
719 results (data not shown). A result is considered to be significant if the corresponding *P* value is below
720 0.05. The analysis has been repeated for the mRNA and protein layer.

721 **Independent cohorts validation**

722 For the validation of Network Component 1, we used published datasets of three PCa cohorts:
723 TCGA, MSKCC, and Aarhus. For TCGA and MSKCC, we downloaded the CNA, mRNA with precomputed z-
724 scores per gene, and corresponding clinical data from cBioPortal[110] (<https://www.cbioportal.org/>).
725 There were 489 samples with \log_2 CNA data and 493 samples with mRNA profiles in TCGA. In MSKCC,
726 there were 157 primary tumors with CNA data and 131 primary tumors with mRNA data. The clinical
727 endpoint used in TCGA was the progression-free survival time and the disease-free survival in MSKCC. All
728 previous samples had known survival time.

729 For the Aarhus study (NCBI GEO dataset GSE46602), we downloaded the mRNA matrix and
730 corresponding clinical information as described in Ycart et al [111]. The resulting mRNA matrix consisted
731 of 20,186 genes and 50 samples- 36 PCa samples with known RFS time and 14 benign samples. Once

732 excluding the benign samples, we computed z-scores per gene in order to have comparable values with
733 the other two studies. These 36 PCa samples were also considered in the subsequent survival analysis.
734 CNA data was not available for the Aarhus study.

735 We reduced all datasets to the nine genes of Network Component 1. In each of the datasets, we
736 computed for each sample an average copy number change (CNA) or an average z-score (mRNA) across
737 the nine genes of Network Component 1 (combined risk score). Subsequently, we used these combined
738 risk scores to split the samples of each dataset into two groups: samples with a combined risk score
739 larger or equal to the median combined risk score of the study were considered as 'altered' and the rest
740 as 'unaltered'. Kaplan-Meier curves were generated for the two groups. Due to the high level of
741 discretized values in MSKCC at the CNA layer, a sample is considered to be 'altered' in that dataset if its
742 combined risk score is above zero.

743 Additionally, we fitted for each dataset a Cox proportional-hazards model to predict survival
744 time using as input variables the average copy number change (CNA) or average z-score (mRNA) of
745 Network Component 1 (variable of interest) and the age (when available, *i.e.* for TCGA and Aarhus). For
746 each dataset with available copy number information (*i.e.* for the TCGA and MSKCC studies), we fitted a
747 second Cox proportional-hazards model with the fraction of genome altered as an additional input
748 variable. For the model fitting, we used the R package survival (<https://cran.r-project.org/web/packages/survival/index.html>).

750 Analysis of regulators and target genes

751 For this analysis, we used once again the STRING gene interaction network. For each target gene
752 (AGR2, ACPP, POSTN, LGALS3BP), we split the network nodes into two groups as follows: firstly we
753 identified the neighbors of the target gene supported by a combined evidence larger than 0.2. This set
754 together with the target gene constituted group 1 while the remaining network nodes constituted group
755 2. For this splitting, only genes present in the network with copy number measurements and with a
756 matching STRING identifier (**Additional file 7: Table S6**) were considered (*i.e.* 17,306 genes in total).
757 Subsequently, genes altered (*i.e.* with \log_2 copy number ratio greater than 0.5 in absolute) in fewer than
758 four tumor samples across the 66 tumor samples were filtered out in each of the two groups. Genes in
759 group 1 after the CNA filtering are potential regulators of the target under consideration. For each gene
760 in the two groups after the filtering, we computed the Spearman correlation between its CNAs and the
761 mRNA FCs of the target gene. For computing the correlation, the samples were reduced to the 63 tumor
762 samples with available mRNA data.

763 Subsequently, we fitted an elastic net model with alpha=0.5 for ACPP. We used as output
764 variable the mRNA FC of ACPP and as input variables the CNAs of the genes in group 1 after the copy
765 number event filtering. The value for the regularization parameter lambda was chosen through 10-fold
766 cross validation (default in the R package glmnet (<https://cran.r-project.org/web/packages/glmnet/>)).
767 The samples were necessarily reduced to the 63 mRNA tumor samples. Predictors/regulators with a non-
768 zero beta coefficient were deemed significant. We have used the elastic net model with alpha=0.5
769 because it is a method giving sparse solutions and can deal with correlated predictors at the same time.

770 As an additional validation to our approach, we used the two independent PCa cohorts
771 described above (TCGA and MSKCC) and reduced the samples to those having both CNA and mRNA
772 profile. This resulted in 488 samples for TCGA and 109 samples for MSKCC. Next, for each of the
773 significant regulators/predictors we computed the Spearman correlation between its CNAs and the
774 corresponding mRNA z-scores of ACPP in each of the two independent studies and checked if the sign of
775 the Spearman correlation matched the sign of the Spearman correlation computed for our cohort, *i.e.*
776 there was an agreement regarding the direction of the association.

777 **Declarations**

778 **Ethics approval and consent to participate**

779 This study was approved by the Cantonal Ethics Committee of Zurich (KEK-ZH-No. 2008-0040), the
780 associated methods were carried out in accordance with the approved guidelines, and each patient has
781 signed an informed consent form.

782 **Consent for publication**

783 Not applicable.

784 **Availability of data and materials**

785 Exome and RNA sequencing data were submitted to the Sequence Read Archive (SRA) at NCBI under
786 accession numbers PRJNA577801 (exome-seq) and PRJNA579899 (RNA-seq), respectively. The SWATH
787 proteomics data were deposited in PRIDE. Project accession code is PXD004589. The published datasets
788 of the two PCa cohorts (TCGA and MSKCC) analyzed during the current study can be downloaded from
789 cBioPortal[110] while the third (Aarhus) is available at the NCBI GEO repository under the accession
790 number GSE46602 .

791 Competing interests

792 R.A. holds shares of Biognosys AG, which operates in the field covered by the article. The research
793 groups of R.A. and T.G. are supported by SCIE, which provides access to prototype instrumentation, and
794 Pressure Biosciences Inc., which provides access to advanced sample preparation instrumentation.

795 Funding

796 This work was supported by the SystemsX.ch project PhosphoNet PPM (to R.A. and P.J.W.), the Swiss
797 National Science Foundation (grant no. 3100A0-688 107679 to R.A.), the European Research Council
798 (grant no. ERC-2008-AdG 233226 and ERC-2014-AdG670821 to R.A.), the Foundation for Scientific
799 Research at the University of Zurich (to P.J.W.), the Westlake Startup Grant (to T.G.), Zhejiang Provincial
800 Natural Science Foundation of China (Grant No. LR19C050001 to T.G.), Hangzhou Agriculture and Society
801 Advancement Program (Grant No. 20190101A04 to T.G.). A.B. and K.C. are supported by the German
802 Federal Ministry of Education and Research Grants Sybacol and PhosphoNetPPM.

803 Authors' contributions

804 A.B., T.G., P.J.W. and R.A. designed the project. P.J.W., T.G., Q.Z., C.E.F., N.J.R., A.C, D.R, J.H.R., C.F., K.S.,
805 C.P., T.H., A.L.M. and C.B. procured the samples and performed the experiments. K.C., T.G., Q.Z., U.W.,
806 R.S., N.C.T, K.O., L.C., L.M., M.R.M, M.M and A.B. designed and performed the statistical analyses with
807 critical inputs from C.Y., H.C., Q.Z., Y.Z., M.H. and other authors. K.C., A.B., T.G. and R.A. interpreted the
808 results. K.C., T.G., P.J.W., A.B. and R.A. wrote the manuscript with inputs from all co-authors. A.B., R.A.,
809 P.J.W. and T.G. supported and supervised the project.

810 Acknowledgements

811 Not applicable.

812 Supplementary information

813 **Additional file 1: Supplementary text and supplementary figures.**

814 **Additional file 2: Table S1. Clinicopathological, immunological and other molecular information of the**
815 **39 PCa patients.** (a) Overall clinicopathological characteristics. (b) Detailed information for each patient.
816 Pat: numeric patient ID; Pat_id: patient ID grouped by the overall grade. L: low grade; M: intermediate
817 grade; H: high grade; Overall_Gleason_GrGp: overall ISUP grade group; pT: tumor stage; pN: nodal

818 status; R: surgical margin status; Age_at_OP: age at operation; PSA_at_Diag: blood PSA level at
819 diagnosis; Time (months): RFS time. A value of 0 corresponds to patients excluded for the reasons
820 explained in the '**Methods**' section (see 'Patients and samples'); Status: status indicator. 1 means
821 recurrence; DX name: tissue region name; ImageName: name of the scanned images; index_tumor_id:
822 patient ID of TA1 (or TA); TA1_GrGp: grade group for TA1; T_GrGp: grade group for TA2.

823 **Additional file 3: Table S2. Exome analysis of the peripheral blood cells and 105 prostate tumor**
824 **punches in 39 patients.** (a) Allele frequencies (AF) of somatic single nucleotide variants (SNVs) that were
825 called by our bioinformatics pipeline. Genes with called SNV are indicated by an AF > 0. A value of 0
826 indicates that no SNV was found in the respective genes. In our data, no gene was found with more than
827 one called somatic SNV. (b) Number of samples per gene with called somatic SNV. (c) Protein domain
828 analysis using DAVID.

829 **Additional file 4: Table S3. Copy number analysis of 105 PCa samples.** (a) Log₂ ratios indicating the CNA
830 status are shown for all genes in all samples. Values were determined by overlapping gene locations with
831 CNA segments as calculated by CopywriteR. In case more than one segment overlapped with a gene,
832 number was chosen that had the highest absolute value. (b) Genes are shown with log₂ ratios higher
833 than 0.5 or lower than -0.5 in at least one sample.

834 **Additional file 5: Table S4. RNA-seq analysis.** (a) Log₂FCs (relative to all benign samples) for all genes
835 across the tumor samples. (b) mRIN score per sample generated using mRIN (v1.2.0). (c) ETS family gene
836 fusions observed in tumor samples using FusionCatcher: a value of 1 means that the fusion was observed
837 in the respective sample but not its corresponding benign sample, otherwise the value is 0. (d)
838 Normalized RNA-seq count data matrix.

839 **Additional file 6: Table S5. Proteomics data of 210 PCa samples with duplicates.** (a) Sample information
840 includes patient ID, clinical diagnosis, sample ID and batch design. (b) Protein matrix of log₂ scaled
841 intensity of 2,371 proteins quantified in 210 PCa samples.

842 **Additional file 7: Table S6. Integration analysis of 66 tumor samples.** (a) Information (i.e. reference
843 linking them to PCa, consistency between observed and reported effect and number of tumor samples
844 with CNAs) for the first 10 highest-scoring proteins (those with largest average absolute FCs across all
845 tumor specimens). (b) Consistently up-regulated genes in the high-grade tumors: for each of these
846 genes, there is a significant up-regulation of its FCs after network smoothing in the group G4/5
847 compared to the group G1 in all three layers (CNA, mRNA and protein). (c) Consistently down-regulated

848 genes in the high-grade tumors: for each of these genes, there is a significant down-regulation of its FCs
849 after network smoothing in the group G4/5 compared to the group G1 in all three layers (CNA, mRNA
850 and protein). (d) Chromosome information for the gene members of Network Component 1. (e)
851 Mapping from gene symbols to STRING identifiers.

852 References

853

854 1. Ferlay J, Soerjomataram I, Dikshit R, Eser S, Mathers C, Rebelo M, Parkin DM, Forman D, Bray F:
855 **Cancer incidence and mortality worldwide: sources, methods and major patterns in**
856 **GLOBOCAN 2012.** *Int J Cancer* 2015, **136**:E359-386.

857 2. Epstein JI, Zlelfsky MJ, Sjoberg DD, Nelson JB, Egevad L, Magi-Galluzzi C, Vickers AJ, Parwani AV,
858 Reuter VE, Fine SW, et al: **A Contemporary Prostate Cancer Grading System: A Validated**
859 **Alternative to the Gleason Score.** *Eur Urol* 2016, **69**:428-435.

860 3. Gordetsky J, Epstein J: **Grading of prostatic adenocarcinoma: current state and prognostic**
861 **implications.** *Diagn Pathol* 2016, **11**:25.

862 4. Berger MF, Lawrence MS, Demichelis F, Drier Y, Cibulskis K, Sivachenko AY, Sboner A, Esgueva R,
863 Pflueger D, Sougnez C, et al: **The genomic complexity of primary human prostate cancer.**
864 *Nature* 2011, **470**:214-220.

865 5. Barbieri CE, Baca SC, Lawrence MS, Demichelis F, Blattner M, Theurillat JP, White TA, Stojanov P,
866 Van Allen E, Stransky N, et al: **Exome sequencing identifies recurrent SPOP, FOXA1 and MED12**
867 **mutations in prostate cancer.** *Nat Genet* 2012, **44**:685-689.

868 6. Robinson D, Van Allen EM, Wu YM, Schultz N, Lonigro RJ, Mosquera JM, Montgomery B, Taplin
869 ME, Pritchard CC, Attard G, et al: **Integrative clinical genomics of advanced prostate cancer.** *Cell*
870 2015, **161**:1215-1228.

871 7. Baca SC, Prandi D, Lawrence MS, Mosquera JM, Romanel A, Drier Y, Park K, Kitabayashi N,
872 MacDonald TY, Ghandi M, et al: **Punctuated evolution of prostate cancer genomes.** *Cell* 2013,
873 **153**:666-677.

874 8. Cancer Genome Atlas Research N: **The Molecular Taxonomy of Primary Prostate Cancer.** *Cell*
875 2015, **163**:1011-1025.

876 9. Wedge DC, Gundem G, Mitchell T, Woodcock DJ, Martincorena I, Ghori M, Zamora J, Butler A,
877 Whitaker H, Kote-Jarai Z, et al: **Sequencing of prostate cancers identifies new cancer genes,**
878 **routes of progression and drug targets.** *Nat Genet* 2018, **50**:682-692.

879 10. Tomlins SA, Rhodes DR, Perner S, Dhanasekaran SM, Mehra R, Sun XW, Varambally S, Cao X,
880 Tchinda J, Kuefer R, et al: **Recurrent fusion of TMPRSS2 and ETS transcription factor genes in**
881 **prostate cancer.** *Science* 2005, **310**:644-648.

882 11. Grasso CS, Wu YM, Robinson DR, Cao X, Dhanasekaran SM, Khan AP, Quist MJ, Jing X, Lonigro RJ,
883 Brenner JC, et al: **The mutational landscape of lethal castration-resistant prostate cancer.**
884 *Nature* 2012, **487**:239-243.

885 12. Boutros PC, Fraser M, Harding NJ, de Borja R, Trudel D, Lalonde E, Meng A, Hennings-Yeomans
886 PH, McPherson A, Sabelnykova VY, et al: **Spatial genomic heterogeneity within localized,**
887 **multifocal prostate cancer.** *Nat Genet* 2015, **47**:736-745.

888 13. Cooper CS, Eeles R, Wedge DC, Van Loo P, Gundem G, Alexandrov LB, Kremeyer B, Butler A,
889 Lynch AG, Camacho N, et al: **Analysis of the genetic phylogeny of multifocal prostate cancer**
890 **identifies multiple independent clonal expansions in neoplastic and morphologically normal**
891 **prostate tissue.** *Nat Genet* 2015, **47**:367-372.

892 14. Lovf M, Zhao S, Axcrona U, Johannessen B, Bakken AC, Carm KT, Hoff AM, Myklebost O, Meza-
893 Zepeda LA, Lie AK, et al: **Multifocal Primary Prostate Cancer Exhibits High Degree of Genomic**
894 **Heterogeneity.** *Eur Urol* 2019, **75**:498-505.

895 15. Lindberg J, Klevebring D, Liu W, Neiman M, Xu J, Wiklund P, Wiklund F, Mills IG, Egevad L,
896 Gronberg H: **Exome sequencing of prostate cancer supports the hypothesis of independent**
897 **tumour origins.** *Eur Urol* 2013, **63**:347-353.

898 16. Espiritu SMG, Liu LY, Rubanova Y, Bhandari V, Holgersen EM, Szyca LM, Fox NS, Chua MLK,
899 Yamaguchi TN, Heisler LE, et al: **The Evolutionary Landscape of Localized Prostate Cancers**
900 **Drives Clinical Aggression.** *Cell* 2018, **173**:1003-1013 e1015.

901 17. Sinha A, Huang V, Livingstone J, Wang J, Fox NS, Kurganova N, Ignatchenko V, Fritsch K, Donmez
902 N, Heisler LE, et al: **The Proteogenomic Landscape of Curable Prostate Cancer.** *Cancer Cell* 2019,
903 **35**:414-427 e416.

904 18. Latonen L, Afyounian E, Jylha A, Nattinen J, Aapola U, Annala M, Kivinummi KK, Tammela TTL,
905 Beuerman RW, Uusitalo H, et al: **Integrative proteomics in prostate cancer uncovers robustness**
906 **against genomic and transcriptomic aberrations during disease progression.** *Nat Commun*
907 2018, **9**:1176.

908 19. Iglesias-Gato D, Wikstrom P, Tyanova S, Lavallee C, Thysell E, Carlsson J, Hagglof C, Cox J, Andren
909 O, Stattin P, et al: **The Proteome of Primary Prostate Cancer.** *Eur Urol* 2016, **69**:942-952.

910 20. Attard G, Parker C, Eeles RA, Schroder F, Tomlins SA, Tannock I, Drake CG, de Bono JS: **Prostate**
911 **cancer.** *Lancet* 2016, **387**:70-82.

912 21. Goncalves E, Fragoulis A, Garcia-Alonso L, Cramer T, Saez-Rodriguez J, Beltrao P: **Widespread**
913 **Post-transcriptional Attenuation of Genomic Copy-Number Variation in Cancer.** *Cell Syst* 2017,
914 **5**:386-398 e384.

915 22. Liu Y, Beyer A, Aebersold R: **On the Dependency of Cellular Protein Levels on mRNA**
916 **Abundance.** *Cell* 2016, **165**:535-550.

917 23. Guo T, Kouvonen P, Koh CC, Gillet LC, Wolski WE, Rost HL, Rosenberger G, Collins BC, Blum LC,
918 Gillessen S, et al: **Rapid mass spectrometric conversion of tissue biopsy samples into**
919 **permanent quantitative digital proteome maps.** *Nat Med* 2015, **21**:407-413.

920 24. Guo T, Li L, Zhong Q, Rupp NJ, Charmpi K, Wong CE, Wagner U, Rueschoff JH, Jochum W,
921 Fankhauser CD, et al: **Multi-region proteome analysis quantifies spatial heterogeneity of**
922 **prostate tissue biomarkers.** *Life Sci Alliance* 2018, **1**.

923 25. Umbehr M, Kessler TM, Sulser T, Kristiansen G, Probst N, Steurer J, Bachmann LM: **ProCOC: the**
924 **prostate cancer outcomes cohort study.** *BMC Urol* 2008, **8**:9.

925 26. Wettstein MS, Saba K, Umbehr MH, Murtola TJ, Fankhauser CD, Adank JP, Hofmann M, Sulser T,
926 Hermanns T, Moch H, et al: **Prognostic Role of Preoperative Serum Lipid Levels in Patients**
927 **Undergoing Radical Prostatectomy for Clinically Localized Prostate Cancer.** *Prostate* 2017,
928 **77**:549-556.

929 27. Epstein JI, Egevad L, Amin MB, Delahunt B, Srigley JR, Humphrey PA, Grading C: **The 2014**
930 **International Society of Urological Pathology (ISUP) Consensus Conference on Gleason Grading**
931 **of Prostatic Carcinoma: Definition of Grading Patterns and Proposal for a New Grading System.**
932 *Am J Surg Pathol* 2016, **40**:244-252.

933 28. Epstein JI, Amin MB, Reuter VE, Humphrey PA: **Contemporary Gleason Grading of Prostatic**
934 **Carcinoma: An Update With Discussion on Practical Issues to Implement the 2014**
935 **International Society of Urological Pathology (ISUP) Consensus Conference on Gleason Grading**
936 **of Prostatic Carcinoma.** *Am J Surg Pathol* 2017, **41**:e1-e7.

937 29. DeMarzo AM, Nelson WG, Isaacs WB, Epstein JI: **Pathological and molecular aspects of prostate**
938 **cancer.** *Lancet* 2003, **361**:955-964.

939 30. Reznik E, Sander C: **Extensive decoupling of metabolic genes in cancer.** *PLoS Comput Biol* 2015,
940 **11**:e1004176.

941 31. Taylor BS, Schultz N, Hieronymus H, Gopalan A, Xiao Y, Carver BS, Arora VK, Kaushik P, Cerami E,
942 Reva B, et al: **Integrative genomic profiling of human prostate cancer.** *Cancer Cell* 2010, **18**:11-
943 22.

944 32. Zhang B, Wang J, Wang X, Zhu J, Liu Q, Shi Z, Chambers MC, Zimmerman LJ, Shaddox KF, Kim S,
945 et al: **Proteogenomic characterization of human colon and rectal cancer.** *Nature* 2014, **513**:382-
946 387.

947 33. Geiger T, Cox J, Mann M: **Proteomic changes resulting from gene copy number variations in**
948 **cancer cells.** *PLoS Genet* 2010, **6**:e1001090.

949 34. Juschke C, Dohnal I, Pichler P, Harzer H, Swart R, Ammerer G, Mechtler K, Knoblich JA:
950 **Transcriptome and proteome quantification of a tumor model provides novel insights into**
951 **post-transcriptional gene regulation.** *Genome Biol* 2013, **14**:r133.

952 35. Stingle S, Stoehr G, Peplowska K, Cox J, Mann M, Storchova Z: **Global analysis of genome,**
953 **transcriptome and proteome reveals the response to aneuploidy in human cells.** *Mol Syst Biol*
954 2012, **8**:608.

955 36. Hofree M, Shen JP, Carter H, Gross A, Ideker T: **Network-based stratification of tumor**
956 **mutations.** *Nat Methods* 2013, **10**:1108-1115.

957 37. Zhang JS, Gong A, Cheville JC, Smith DL, Young CY: **AGR2, an androgen-inducible secretory**
958 **protein overexpressed in prostate cancer.** *Genes Chromosomes Cancer* 2005, **43**:249-259.

959 38. Liu Q, Harvey CT, Geng H, Xue C, Chen V, Beer TM, Qian DZ: **Malate dehydrogenase 2 confers**
960 **docetaxel resistance via regulations of JNK signaling and oxidative metabolism.** *Prostate* 2013,
961 **73**:1028-1037.

962 39. Yang J, Song H, Chen L, Cao K, Zhang Y, Li Y, Hao X: **Integrated analysis of microfibrillar-**
963 **associated proteins reveals MFAP4 as a novel biomarker in human cancers.** *Epigenomics* 2019,
964 **11**:1635-1651.

965 40. Senga S, Kobayashi N, Kawaguchi K, Ando A, Fujii H: **Fatty acid-binding protein 5 (FABP5)**
966 **promotes lipolysis of lipid droplets, de novo fatty acid (FA) synthesis and activation of nuclear**
967 **factor-kappa B (NF-kappaB) signaling in cancer cells.** *Biochim Biophys Acta Mol Cell Biol Lipids*
968 2018, **1863**:1057-1067.

969 41. Pan Y, Liu Z, Feng Z, Hui D, Huang X, Tong D, Jin Y: **The overexpression of Rab13 is associated**
970 **with pathogenesis and clinicopathologic variables in hepatocellular carcinoma.** *Tumour Biol*
971 2017, **39**:1010428317696230.

972 42. Zhang W, Sun J, Luo J: **High Expression of Rab-like 3 (Rab13) is Associated with Poor Survival of**
973 **Patients with Non-Small Cell Lung Cancer via Repression of MAPK8/9/10-Mediated**
974 **Autophagy.** *Med Sci Monit* 2016, **22**:1582-1588.

975 43. Szklarczyk D, Franceschini A, Wyder S, Forsslund K, Heller D, Huerta-Cepas J, Simonovic M, Roth A,
976 Santos A, Tsaftou KP, et al: **STRING v10: protein-protein interaction networks, integrated over**
977 **the tree of life.** *Nucleic Acids Research* 2015, **43**:D447-D452.

978 44. Muniyan S, Chaturvedi NK, Dwyer JG, Lagrange CA, Chaney WG, Lin MF: **Human prostatic acid**
979 **phosphatase: structure, function and regulation.** *Int J Mol Sci* 2013, **14**:10438-10464.

980 45. Araujo CL, Quintero IB, Ovaska K, Herrala AM, Hautaniemi S, Vihko PT: **Transmembrane**
981 **prostatic acid phosphatase (TMPAP) delays cells in G1 phase of the cell cycle.** *Prostate* 2016,
982 **76**:151-162.

983 46. Bhatia-Gaur R, Donjacour AA, Sciavolino PJ, Kim M, Desai N, Young P, Norton CR, Gridley T,
984 Cardiff RD, Cunha GR, et al: **Roles for Nkx3.1 in prostate development and cancer.** *Genes Dev*
985 1999, **13**:966-977.

986 47. Gurel B, Ali TZ, Montgomery EA, Begum S, Hicks J, Goggins M, Eberhart CG, Clark DP, Bieberich
987 CJ, Epstein JI, De Marzo AM: **NKX3.1 as a marker of prostatic origin in metastatic tumors.** *Am J*
988 *Surg Pathol* 2010, **34**:1097-1105.

989 48. Oki S, Ohta T, Shioi G, Hatanaka H, Ogasawara O, Okuda Y, Kawaji H, Nakaki R, Sese J, Meno C:
990 **ChIP-Atlas: a data-mining suite powered by full integration of public ChIP-seq data.** *EMBO Rep*
991 2018, **19**.

992 49. Vanunu O, Magger O, Ruppin E, Shlomi T, Sharan R: **Associating Genes and Protein Complexes**
993 **with Disease via Network Propagation.** *Plos Computational Biology* 2010, **6**.

994 50. Zhou D, Bousquet O, Lal TN, Weston J, Schölkopf B: **Learning with Local and Global Consistency.**
995 *Advances in Neural Information Processing Systems* 2004, **16**:312-328.

996 51. Baude A, Aaes TL, Zhai B, Al-Nakouzi N, Oo HZ, Daugaard M, Rohde M, Jaattela M: **Hepatoma-**
997 **derived growth factor-related protein 2 promotes DNA repair by homologous recombination.**
998 *Nucleic Acids Res* 2016, **44**:2214-2226.

999 52. Guler GD, Tindell CA, Pitti R, Wilson C, Nichols K, Kaiwai CT, Kim HJ, Wongchenko M, Yan Y, Haley
1000 **B: Repression of Stress-Induced LINE-1 Expression Protects Cancer Cell Subpopulations from**
1001 **Lethal Drug Exposure.** *Cancer Cell* 2017, **32**:221.

1002 53. Slezak J, Truong M, Huang W, Jarrard D: **HP1gamma expression is elevated in prostate cancer**
1003 **and is superior to Gleason score as a predictor of biochemical recurrence after radical**
1004 **prostatectomy.** *BMC Cancer* 2013, **13**:148.

1005 54. Ceol CJ, Yariv H, Judit JV, Steve B, Orlando DA, Valentine B, Lauriane F, Lin WM, Hollmann TJ,
1006 Fabrizio F: **The SETDB1 histone methyltransferase is recurrently amplified in and accelerates**
1007 **melanoma.** *Nature* 2011, **471**:513-517.

1008 55. Sun Y, Wei M, Ren SC, Chen R, Xu WD, Wang FB, Lu J, Shen J, Yu YW, Hou JG, et al: **Histone**
1009 **methyltransferase SETDB1 is required for prostate cancer cell proliferation, migration and**
1010 **invasion.** *Asian J Androl* 2014, **16**:319-324.

1011 56. Luo H, Cowen L, Yu G, Jiang W, Tang Y: **SMG7 is a critical regulator of p53 stability and function**
1012 **in DNA damage stress response.** *Cell Discovery* 2016, **2**:15042.

1013 57. Karanika S, Karantanios T, Li L, Wang J, Park S, Yang G, Zuo X, Song JH, Maity SN, Manyam GC:
1014 **Targeting DNA Damage Response in Prostate Cancer by Inhibiting Androgen Receptor-CDC6-**
1015 **ATR-Chk1 Signaling.** *Cell Reports* 2017, **18**:1970.

1016 58. Diouf B, Cheng Q, Krynetskaia NF, Yang W, Cheok M, Pei D, Fan Y, Cheng C, Krynetskiy EY, Geng
1017 **H: Somatic deletions of genes regulating MSH2 protein stability cause DNA mismatch repair**
1018 **deficiency and drug resistance in human leukemia cells.** *Nature Medicine* 2011, **17**:1298-1303.

1019 59. Yao S, Bee A, Brewer D, Dodson A, Beesley C, Ke Y, Ambroisine L, Fisher G, Møller H, Dickinson T:
1020 **PRKC-ζ Expression Promotes the Aggressive Phenotype of Human Prostate Cancer Cells and Is**
1021 **a Novel Target for Therapeutic Intervention.** *Genes Cancer* 2010, **1**:444-464.

1022 60. Zhou W, Jiang Y, Zhu M, Hang D, Chen J, Zhou J, Dai J, Ma H, Hu Z, Jin G, et al: **Low-frequency**
1023 **nonsynonymous variants in FKBPL and ARPC1B genes are associated with breast cancer risk in**
1024 **Chinese women.** *Mol Carcinog* 2017, **56**:774-780.

1025 61. De Robertis M, Mazza T, Fusilli C, Loiacono L, Poeta ML, Sanchez M, Massi E, Lamorte G, Diodoro
1026 MG, Pescarmona E, et al: **EphB2 stem-related and EphA2 progression-related miRNA-based**
1027 **networks in progressive stages of CRC evolution: clinical significance and potential miRNA**
1028 **drivers.** *Mol Cancer* 2018, **17**:169.

1029 62. Zeng Z, Yang H, Xiao S: **ACTL6A expression promotes invasion, metastasis and epithelial**
1030 **mesenchymal transition of colon cancer.** *BMC Cancer* 2018, **18**:1020.

1031 63. Castro MA, Dal-Pizzol F, Zdanov S, Soares M, Muller CB, Lopes FM, Zanotto-Filho A, da Cruz
1032 Fernandes M, Moreira JC, Shacter E, Klamt F: **CFL1 expression levels as a prognostic and drug**
1033 **resistance marker in nonsmall cell lung cancer.** *Cancer* 2010, **116**:3645-3655.

1034 64. Overbye A, Skotland T, Koehler CJ, Thiede B, Seierstad T, Berge V, Sandvig K, Llorente A:
1035 **Identification of prostate cancer biomarkers in urinary exosomes.** *Oncotarget* 2015, **6**:30357-
1036 30376.

1037 65. Deng Z, Wan M, Cao P, Rao A, Cramer SD, Sui G: **Yin Yang 1 regulates the transcriptional activity**
1038 **of androgen receptor.** *Oncogene* 2009, **28**:3746-3757.

1039 66. Fournier PG, Juarez P, Jiang G, Clines GA, Niewolna M, Kim HS, Walton HW, Peng XH, Liu Y,
1040 Mohammad KS, et al: **The TGF-beta Signaling Regulator PMEPA1 Suppresses Prostate Cancer**
1041 **Metastases to Bone.** *Cancer Cell* 2015, **27**:809-821.

1042 67. Yang J, Lu C, Wei J, Guo Y, Liu W, Luo L, Fisch G, Li X: **Inhibition of KPNA4 attenuates prostate**
1043 **cancer metastasis.** *Oncogene* 2017, **36**:2868-2878.

1044 68. Liu W, Xie CC, Zhu Y, Li T, Sun J, Cheng Y, Ewing CM, Dalrymple S, Turner AR, Sun J, et al:
1045 **Homozygous deletions and recurrent amplifications implicate new genes involved in prostate**
1046 **cancer.** *Neoplasia* 2008, **10**:897-907.

1047 69. Trasino SE, Harrison EH, Wang TT: **Androgen regulation of aldehyde dehydrogenase 1A3**
1048 **(ALDH1A3) in the androgen-responsive human prostate cancer cell line LNCaP.** *Exp Biol Med*
1049 (*Maywood*) 2007, **232**:762-771.

1050 70. Bonaccorsi L, Luciani P, Nesi G, Mannucci E, Deledda C, Dichiara F, Paglierani M, Rosati F, Masieri
1051 L, Serni S, et al: **Androgen receptor regulation of the seladin-1/DHCR24 gene: altered**
1052 **expression in prostate cancer.** *Lab Invest* 2008, **88**:1049-1056.

1053 71. Li H, Xiao D, Hu L, He T: **Association of CYP1A1 polymorphisms with prostate cancer risk: an**
1054 **updated meta-analysis.** *Mol Biol Rep* 2012, **39**:10273-10284.

1055 72. Aktas D, Hascicek M, Sozen S, Ozen H, Tuncbilek E: **CYP1A1 and GSTM1 polymorphic genotypes**
1056 **in patients with prostate cancer in a Turkish population.** *Cancer Genet Cytogenet* 2004, **154**:81-
1057 85.

1058 73. Acevedo C, Opazo JL, Huidobro C, Cabezas J, Iturrieta J, Quinones Sepulveda L: **Positive**
1059 **correlation between single or combined genotypes of CYP1A1 and GSTM1 in relation to**
1060 **prostate cancer in Chilean people.** *Prostate* 2003, **57**:111-117.

1061 74. Cao HM, Wan Z, Wu Y, Wang HY, Guan C: **Development and internal validation of a novel**
1062 **model and markers to identify the candidates for lymph node metastasis in patients with**
1063 **prostate cancer.** *Medicine (Baltimore)* 2019, **98**:e16534.

1064 75. Kawamura N, Nimura K, Saga K, Ishibashi A, Kitamura K, Nagano H, Yoshikawa Y, Ishida K,
1065 Nonomura N, Arisawa M, et al: **SF3B2-Mediated RNA Splicing Drives Human Prostate Cancer**
1066 **Progression.** *Cancer Res* 2019, **79**:5204-5217.

1067 76. Wen M, Kwon Y, Wang Y, Mao JH, Wei G: **Elevated expression of UBE2T exhibits oncogenic**
1068 **properties in human prostate cancer.** *Oncotarget* 2015, **6**:25226-25239.

1069 77. Kleppe A, Albregtsen F, Vlatkovic L, Pradhan M, Nielsen B, Hveem TS, Askautrud HA, Kristensen
1070 GB, Nesbakken A, Trovik J, et al: **Chromatin organisation and cancer prognosis: a pan-cancer**
1071 **study.** *Lancet Oncol* 2018, **19**:356-369.

1072 78. Lee RS, Roberts CW: **Linking the SWI/SNF complex to prostate cancer.** *Nat Genet* 2013,
1073 **45**:1268-1269.

1074 79. Chuu C-P, Lin C-Y, Huang S-H, Tsai KK-C: **MO2-10-6ACTL6A is a novel oncogene and prognostic**
1075 **biomarker for prostate cancer.** *Annals of Oncology* 2019, **30**.

1076 80. Doyon Y, Selleck W, Lane WS, Tan S, Cote J: **Structural and functional conservation of the NuA4**
1077 **histone acetyltransferase complex from yeast to humans.** *Mol Cell Biol* 2004, **24**:1884-1896.

1078 81. Cai Y, Jin J, Florens L, Swanson SK, Kusch T, Li B, Workman JL, Washburn MP, Conaway RC,
1079 Conaway JW: **The mammalian YL1 protein is a shared subunit of the TRRAP/TIP60 histone**
1080 **acetyltransferase and SRCAP complexes.** *J Biol Chem* 2005, **280**:13665-13670.

1081 82. Mortensen MM, Hoyer S, Lynnerup AS, Orntoft TF, Sorensen KD, Borre M, Dyrskjot L: **Expression**
1082 **profiling of prostate cancer tissue delineates genes associated with recurrence after**
1083 **prostatectomy.** *Sci Rep* 2015, **5**:16018.

1084 83. Hussain M, Mateo J, Fizazi K, Saad F, Shore ND, Sandhu S, Chi KN, Sartor O, Agarwal N, Olmos D,
1085 et al: **LBA12_PRPROfound: Phase III study of olaparib versus enzalutamide or abiraterone for**

1086 **metastatic castration-resistant prostate cancer (mCRPC) with homologous recombination**
1087 **repair (HRR) gene alterations.** *Annals of Oncology* 2019, **30**.

1088 84. Langmead B, Salzberg SL: **Fast gapped-read alignment with Bowtie 2.** *Nat Methods* 2012, **9**:357-
1089 359.

1090 85. McKenna A, Hanna M, Banks E, Sivachenko A, Cibulskis K, Kernytsky A, Garimella K, Altshuler D,
1091 Gabriel S, Daly M, DePristo MA: **The Genome Analysis Toolkit: a MapReduce framework for**
1092 **analyzing next-generation DNA sequencing data.** *Genome Res* 2010, **20**:1297-1303.

1093 86. Bolger AM, Lohse M, Usadel B: **Trimmomatic: a flexible trimmer for Illumina sequence data.**
1094 *Bioinformatics* 2014, **30**:2114-2120.

1095 87. Li H, Handsaker B, Wysoker A, Fennell T, Ruan J, Homer N, Marth G, Abecasis G, Durbin R,
1096 Genome Project Data Processing S: **The Sequence Alignment/Map format and SAMtools.**
1097 *Bioinformatics* 2009, **25**:2078-2079.

1098 88. Quinlan AR, Hall IM: **BEDTools: a flexible suite of utilities for comparing genomic features.**
1099 *Bioinformatics* 2010, **26**:841-842.

1100 89. Cibulskis K, Lawrence MS, Carter SL, Sivachenko A, Jaffe D, Sougnez C, Gabriel S, Meyerson M,
1101 Lander ES, Getz G: **Sensitive detection of somatic point mutations in impure and**
1102 **heterogeneous cancer samples.** *Nat Biotechnol* 2013, **31**:213-219.

1103 90. Saunders CT, Wong WSW, Swamy S, Becq J, Murray LJ, Cheetham RK: **Strelka: accurate somatic**
1104 **small-variant calling from sequenced tumor-normal sample pairs.** *Bioinformatics* 2012,
1105 **28**:1811-1817.

1106 91. Sherry ST, Ward MH, Kholodov M, Baker J, Phan L, Smigelski EM, Sirotnik K: **dbSNP: the NCBI**
1107 **database of genetic variation.** *Nucleic Acids Res* 2001, **29**:308-311.

1108 92. Kuilman T, Velds A, Kemper K, Ranzani M, Bombardelli L, Hoogstraat M, Nevedomskaya E, Xu G,
1109 de Ruiter J, Lolkema MP, et al: **CopywriteR: DNA copy number detection from off-target**
1110 **sequence data.** *Genome Biol* 2015, **16**:49.

1111 93. Noske A, Brandt S, Valtcheva N, Wagner U, Zhong Q, Bellini E, Fink D, Obermann EC, Moch H,
1112 Wild PJ: **Detection of CCNE1/URI (19q12) amplification by in situ hybridisation is common in**
1113 **high grade and type II endometrial cancer.** *Oncotarget* 2017, **8**:14794-14805.

1114 94. Dobin A, Davis CA, Schlesinger F, Drenkow J, Zaleski C, Jha S, Batut P, Chaisson M, Gingeras TR:
1115 **STAR: ultrafast universal RNA-seq aligner.** *Bioinformatics* 2013, **29**:15-21.

1116 95. Hartley SW, Mullikin JC: **QoRTs: a comprehensive toolset for quality control and data**
1117 **processing of RNA-Seq experiments.** *BMC Bioinformatics* 2015, **16**:224.

1118 96. Feng H, Zhang X, Zhang C: **mRIN for direct assessment of genome-wide and gene-specific mRNA**
1119 **integrity from large-scale RNA-sequencing data.** *Nat Commun* 2015, **6**:7816.

1120 97. Shao W, Guo T, Toussaint NC, Xue P, Wagner U, Li L, Charmpi K, Zhu Y, Wu J, Buljan M, et al:
1121 **Comparative analysis of mRNA and protein degradation in prostate tissues indicates high**
1122 **stability of proteins.** *Nat Commun* 2019, **10**:2524.

1123 98. Sigurgeirsson B, Emanuelsson O, Lundeberg J: **Sequencing degraded RNA addressed by 3' tag**
1124 **counting.** *PLoS One* 2014, **9**:e91851.

1125 99. Liao Y, Smyth GK, Shi W: **featureCounts: an efficient general purpose program for assigning**
1126 **sequence reads to genomic features.** *Bioinformatics* 2014, **30**:923-930.

1127 100. Leek JT, Johnson WE, Parker HS, Jaffe AE, Storey JD: **The sva package for removing batch effects**
1128 **and other unwanted variation in high-throughput experiments.** *Bioinformatics* 2012, **28**:882-
1129 883.

1130 101. Love MI, Huber W, Anders S: **Moderated estimation of fold change and dispersion for RNA-seq**
1131 **data with DESeq2.** *Genome Biol* 2014, **15**:550.

1132 102. Trapnell C, Williams BA, Pertea G, Mortazavi A, Kwan G, van Baren MJ, Salzberg SL, Wold BJ,
1133 Pachter L: **Transcript assembly and quantification by RNA-Seq reveals unannotated transcripts**
1134 **and isoform switching during cell differentiation.** *Nat Biotechnol* 2010, **28**:511-515.

1135 103. Shao S, Guo T, Gross V, Lazarev A, Koh CC, Gillessen S, Joerger M, Jochum W, Aebersold R:
1136 **Reproducible Tissue Homogenization and Protein Extraction for Quantitative Proteomics Using**
1137 **MicroPestle-Assisted Pressure-Cycling Technology.** *J Proteome Res* 2016, **15**:1821-1829.

1138 104. Rosenberger G, Koh CC, Guo T, Rost HL, Kouvolan P, Collins BC, Heusel M, Liu Y, Caron E,
1139 Vichalkovski A, et al: **A repository of assays to quantify 10,000 human proteins by SWATH-MS.**
1140 *Sci Data* 2014, **1**:140031.

1141 105. Röst HL, Rosenberger G, Navarro P, Gillet L, Miladinovic SM, Schubert OT, Wolski W, Collins BC,
1142 Malmstrom J, Malmstrom L, Aebersold R: **OpenSWATH enables automated, targeted analysis of**
1143 **data-independent acquisition MS data.** *Nat Biotechnol* 2014, **32**:219-223.

1144 106. Guo T, Luna A, Rajapakse VN, Koh CC, Wu Z, Liu W, Sun Y, Gao H, Menden MP, Xu C, et al:
1145 **Quantitative Proteome Landscape of the NCI-60 Cancer Cell Lines.** *iScience* 2019, **21**:664-680.

1146 107. Blattmann P, Heusel M, Aebersold R: **SWATH2stats: An R/Bioconductor Package to Process and**
1147 **Convert Quantitative SWATH-MS Proteomics Data for Downstream Analysis Tools.** *PLoS One*
1148 2016, **11**:e0153160.

1149 108. Johnson WE, Li C, Rabinovic A: **Adjusting batch effects in microarray expression data using**
1150 **empirical Bayes methods.** *Biostatistics* 2007, **8**:118-127.

1151 109. Franceschini A, Szklarczyk D, Frankild S, Kuhn M, Simonovic M, Roth A, Lin J, Minguez P, Bork P,
1152 von Mering C, Jensen LJ: **STRING v9.1: protein-protein interaction networks, with increased**
1153 **coverage and integration.** *Nucleic Acids Res* 2013, **41**:D808-815.

1154 110. Gao J, Aksoy BA, Dogrusoz U, Dresdner G, Gross B, Sumer SO, Sun Y, Jacobsen A, Sinha R, Larsson
1155 E, et al: **Integrative analysis of complex cancer genomics and clinical profiles using the**
1156 **cBioPortal.** *Sci Signal* 2013, **6**:pl1.

1157 111. Ycart B, Charmpi K, Rousseaux S, Fournié J-J: **Large scale statistical analysis of GEO datasets.**
1158 2014, **4**:113:111-119.

1159

1160

1161 Figure legends

1162

1163 **Figure 1. Proteogenomics analysis of 105 tissue regions from 39 PCa patients.** **a** Representative
1164 immunohistochemistry images of prostate tissues and the selection of BPH and tumorous tissue regions
1165 for genome, transcriptome and proteome analysis. **b** Kaplan-Meier curves for our cohort when the
1166 patients are stratified by the overall grade (left), the TA1 or TA grade group (middle) and the TA2 or TA
1167 grade group (right). Point-wise 95% confidence bands are shown for the whole range of time values.

1168

1169 **Figure 2. Molecular perturbation scores for point mutations, CNAs, transcriptome and proteome data.**
1170 **a** Distributions of the first type of molecular perturbation scores (DE_count's) for the four grade groups
1171 (visualized as violin plots) at the mutation layer (upper left), CNA layer (upper right), mRNA layer (lower
1172 left) and protein layer (lower right). Points represent the actual values. The horizontal lines correspond
1173 to the median value in each of the four grade groups. **b** Distributions of the second type of molecular
1174 perturbation scores (DE_sum's) for the four grade groups (visualized as violin plots) at the CNA layer
1175 (upper left), mRNA layer (upper right) and protein layer (lower left). Points represent the actual values.
1176 The horizontal lines correspond to the median value in each of the four grade groups. *P* values (in each
1177 of the titles) show the significance of the one-sided Wilcoxon rank sum test where the values of G3 and
1178 G4/5 are gathered together and compared to the values of G1 and G2 (also gathered together).

1179

1180 **Figure 3. Target genes and putative effectors.** **a** Density plots of the FCs in the four grade groups for
1181 three selected proteins (ACPP, POSTN, LGALS3BP) among the 20 highest scoring (score: mean of the
1182 absolute FCs across all tumor samples) proteins. Vertical lines correspond to the average FC in each of
1183 the four grade groups. These proteins were selected as target genes to identify potential regulators. **b**
1184 Distributions of the Spearman correlations of the mRNA target gene FCs with the CNAs of the 'filtered
1185 neighborhood order one' and the 'complement', for the three target genes. The first set/group consists
1186 of the target itself and of those neighbors in STRING with confidence above 0.2, while the second
1187 consists of the remaining network genes in STRING. Both sets are filtered out for genes subject to CNAs
1188 in less than four tumor samples. *P* values (in each of the titles) show the significance of the one-sided t-
1189 test. **c** Heatmap of the CNA matrix reduced to the significant regulators of the target gene ACPP output
1190 by the fitted elastic net model (*i.e.* those with a non-zero beta coefficient). The columns are ordered
1191 based on the grade group while there is a hierarchical clustering of the rows. The added colorbar depicts
1192 the mRNA FCs of the target gene ACPP.

1193

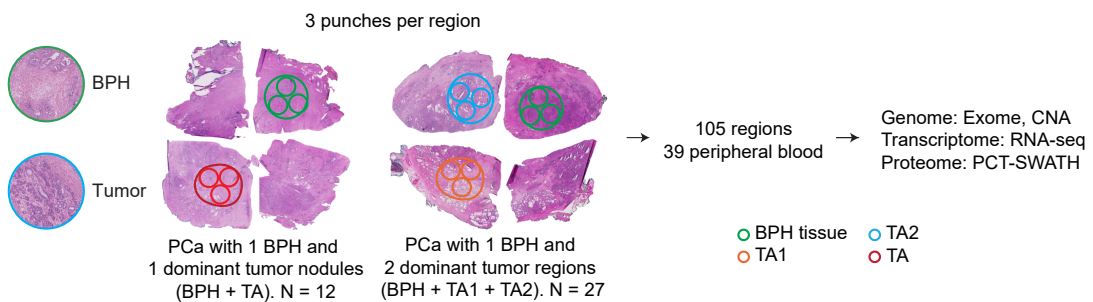
1194 **Figure 4. Cross-omics networks distinguishing high-grade from low-grade tumors.** **a** Sub-networks
1195 consistently up-regulated in high-grade (G4/5) compared to low-grade (G1) tumors across all three
1196 layers (CNA, mRNA and protein). **b** Same as in (a) but down-regulated genes. Functional annotation of
1197 the sub-networks in (a) and (b) with more than one node is given. All edges in (a) and (b) are supported
1198 by either experimental or database evidence (STRING evidence ≥ 0.348). **c** CNA, RNA and protein FCs of
1199 Network Component 1 from (a). Samples are ordered by grade group (top bar). T-test results comparing
1200 Network Component 1 members against no change (*i.e.* 0) are shown for each molecular layer along
1201 with the average FC across Network Component 1 members ('effect size'). Black box marks selected
1202 matching samples from patients with G4/5 and G3 tumor areas; *i.e.* tumor sample pairs from identical
1203 patients. Those areas exhibit weak, but common amplifications of Network Component 1 members at

1204 the CNA and RNA layers. mRNA samples in grey were removed due to low RNA quality. Gray bars at the
1205 bottom show the grade group of the patients (low, intermediate, high) where the samples have (mainly)
1206 come from. **d** Kaplan-Meier curves for 'altered' and 'unaltered' samples, where 'altered' is defined as an
1207 effect size greater or equal to the median effect. Results for three independent studies, TCGA (left),
1208 MSKCC (middle) and Aarhus (right) using the corresponding CNA data when available (first row) and
1209 mRNA data (second row). The Cox model P value corresponds to the P value of the variable of interest
1210 (*i.e.* average copy number change (CNA) or average z-score (mRNA) of Network Component 1) from the
1211 fitted Cox model after adjusting for patient age (when available, *i.e.* for TCGA and Aarhus).

1212
1213 **Figure 5. Within-patient similarity at the different layers.** **a** Distributions of the within-group similarities
1214 for the four grade groups (visualized as violin plots) based on the Pearson correlation at the CNA layer
1215 (upper), mRNA layer (middle) and protein layer (lower). A 'violin' with the correlations between TA1 and
1216 paired TA2 for the different patients has been added to all three plots and colored in purple. Points
1217 represent the actual values. The horizontal lines correspond to the median value in each of the groups. P
1218 values from the one-sided Wilcoxon rank sum test comparing the within-patient to the within-group
1219 similarities (where all values from the four groups are gathered together): 8.97e-09 for the CNA, 4.42e-
1220 08 for the mRNA and 6.27e-04 for the protein layer. **b** The correlations between TA1 and paired TA2 for
1221 the different patients at one layer are plotted against the corresponding correlations at another layer for
1222 each pair of layers: mRNA versus CNA (upper), protein versus CNA (middle) and protein versus mRNA
1223 (lower). The points are labeled and colored based on the overall grade in all plots; r : Pearson correlation.

1224

1225

a**b**